

**Finite Element Modelling and Nano-Mechanical
Characterization of Electroless Alloy Coatings**

Thesis submitted in partial fulfilment of the requirement for the degree of

Master of Mechanical Engineering

By **Tarik Hassan**

Examination Roll Number: M4MEC22006

Registration Number: 131754 of 2015-16

UNDER THE GUIDANCE OF

Prof. GAUTAM MAJUMDAR

Department of Mechanical Engineering

Faculty of Engineering & Technology, Jadavpur University

Kolkata – 700032

June- 2022

CERTIFICATE OF APPROVAL

This foregoing thesis is hereby approved as a credible study of an engineering subject carried out and presented in a manner satisfactory to warrant its acceptance as a prerequisite to the degree for which it has been submitted. It is understood that by this approval the undersigned do not endorse or approve any statement made, opinion expressed or conclusion drawn therein but approve the thesis only for the purpose for which it has been submitted.

.....

.....

Committee on the final examination for evaluation of the thesis

Faculty of Engineering and Technology, Jadavpur University

CERTIFICATE OF SUPERVISOR

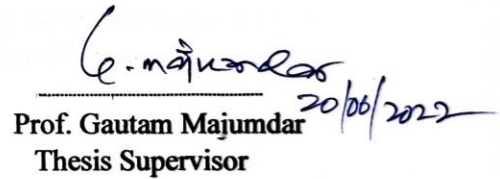
I hereby recommend that the thesis presented under my supervision by Mr Tarik Hassan entitled "Finite Element Modelling and Nano-Mechanical Characterization of Electroless Alloy Coatings" be accepted in partial fulfilment of the requirements for the degree of Master of Mechanical Engineering.

Countersigned by



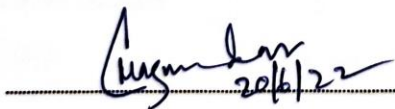
Prof. Amit Karmakar
HOD, Mechanical Engineering

Professor & Head
Dept. of Mechanical Engineering
Jadavpur University, Kolkata-32



Prof. Gautam Majumdar
Thesis Supervisor

Prof. (Dr.) Gautam Majumdar
Professor of Mechanical Engineering
Jadavpur University/Kol-32



Prof. Chandan Mazumdar
Dean of Faculty of Engineering and Technology



DEAN
Faculty of Engineering & Technology
JADAVPUR UNIVERSITY
KOLKATA-700 032

ACKNOWLEDGEMENT

At the very beginning, I would like to owe my hearty gratitude to my esteemed project guide, Prof. Gautam Majumdar, for his continuous help and valuable advice in my work which has enabled me to complete this thesis on time. I am not only thankful to him for only supervising my Master's Thesis work, but also for being a true mentor and guide from the time of my Bachelor of Engineering course at Jadavpur University.

I also acknowledge the important role of Subhasish Da and MD Basiruddin Da, Assistant professor Dept. of Metallurgy and Materials Engineering, JU for helping me to conduct the experiments successfully from external laboratories. With their help, It became possible for me to conduct the Potentiodynamic polarization test, SEM-EDS and Nanoindentation tests from CRF, IEST Shibpur and Dept. of Metallurgy, IIT Kharagpur.

I am indebted to the entire Mechanical Engineering Department, Jadavpur University for providing me with the facilities required during the course of project work. Finally, I would thank my family for being supportive to me in every step of my life which boosts my energy to move forward in my academic and future career life.

Tarik Hassan

Tarik Hassan

Date: 20.06.2022

Contents

Serial No.	Topic	Page No.
	CERTIFICATE OF APPROVAL	02
	CERTIFICATE OF SUPERVISOR	03
	ACKNOWLEDGEMENT	04
1	Research Area	7-12
1.1	Aim and Objective of the Study	7-8
1.2	Literature Review on FEA and some Advanced Properties of Coating and Thin Films	8-10
1.3	Literature Review on Nano-mechanical Characterization of Coating and Thin Films	10-12
1.4	List of Publications in this Field	12
2	Basics of Electroless Nickel Coatings	12-17
2.1	Introduction to Electroless Nickel Coatings	12-13
2.2	Types of Electroless Nickel Coatings	13-14
2.3	Electroless Bath Parameters	14-15
2.4	Properties of Electroless Nickel Coatings	15-17
2.4.1	Surface Roughness	15
2.4.2	Friction and Wear	16
2.4.3	Corrosion Resistance	16
2.4.4	Microstructure and Hardness	16-17
3	Finite Element Analysis	17-31
3.1	Brief Discussion on FEA	17-19
3.2	Application of FEA on Coating-Substrate Assembly	19
3.3	FEA Based Design and Stability Study of Electroless Ni-P Coating Plated over a Stepped Shaft under Thermal Load	20-31
3.3.1	Substrate Preparation and Coating Deposition	20-22
3.3.2	Modelling and Details of FEA	22-24
3.3.2.1	Modelling of Shaft-Coating Assembly	22-23
3.3.2.2	Input details for the Simulation	23-24
3.3.3	Characterization of Electroless Ni-P Coating	25-27
3.3.4	Result and Discussion	27-31
4	Nano-Mechanical Characterization of Electroless Ni-Co-P, Ni-W-P and Ni-Mo-P Alloy Coatings: A Comparative Study	32-41
4.1	Sample Preparation	32-33
4.2	Nanoindentation test on the Coated samples	33-34

4.3	Mathematical Model Used for the Evaluation of Nanomechanical Properties	34-35
4.4	Microstructure and Composition of the Coated Samples	35-38
4.5	Result and Discussion	39-41
5	Optimization of Corrosion Rate of Ni-Co-P Coating Using Box-Behnken Design and Gradient Descent with RMSprop Algorithm	41-50
5.1	Literature review on the Machine Learning Algorithms used for optimization purpose	41-44
5.2	Modelling and Optimization	45-47
5.2.1	Response Surface Modelling(BBD)	45-46
5.2.2	Optimization Using Gradient Descent with RMSprop	46-47
5.3	Results	47-50
5.3.1	Analysis of variance for response surface	47-48
5.3.2	Machine learning optimization result	48-50
6	Conclusion	50-51
7	Future Scope	51-52
8	References	52-61

1. Research Area

1.1. Aim and Objective of the Study

In this present theoretical and experimental research, the main objective is divided into three parts. The first one is based on Ansys modelling of coating-substrate assembly, the second one is Nanoindentation study on three different electroless coatings and the last one is based on Machine learning modelling and optimization of corrosion rate of Ni-Co-P coating.

Objective I

The main motive behind this study is to perform the modelling of Ni-P coating and the substrate assembly using the finite element analysis framework. Coating having a thickness of 50 μ m is applied over a stepped shaft made of stainless steel and analysed in Ansys Workbench. Considering the immense use of several mechanical systems at elevated temperatures, the coated shaft is studied in a hot environment of temperature 200°C. The thermal effect on the system is studied and results are discussed in detail with respective figures. Elastic modulus of Ni-P coating required for the analysis is evaluated from the nanoindentation test under 10mN load. The analysis focuses on the evaluation of the critical design parameters like equivalent stress, total deformation, strain energy and thermal strain over the entire body. Along with the evaluation of the said parameters, four separate paths are created on the model to study the difference of induced stress and strain energy between the contacting surfaces of the shaft and the coating. It is found that there is a sharp discontinuity in these values and this discontinuity is further interpreted as a measure of the stability of coating over the substrate. It is found that the higher the difference of stress and strain energy lower is the stability of the assembly which is considered to be realistic and in accordance with the elasticity principles. Present study is expected to be very helpful to check the application-based feasibility of coatings and thin films which might be very cumbersome and erroneous when assessed by an experimental study due to the very low thickness value.

Objective II

Nanoindentation is an efficient method to evaluate some crucial mechanical properties of thin films and coatings as it is capable of indenting the outer thin layer without affecting the substrate material. In this study, nickel-phosphorous-based cobalt, tungsten and molybdenum coatings are synthesized by electroless deposition. The Vicker's nanohardness and elastic modulus of the coatings are evaluated through nanoindentation tests performed by a regular Berkovich indenter under a peak load of 10mN. Elastic modulus is approximated from the load-displacement data of the indenter using the Oliver-Pharr mathematical model while the hardness is calculated by dividing the load by the indentation area. For each sample, indentation is performed at five different locations to enhance the accuracy of the estimated values. As the properties are highly dependent on the composition and quality of the deposition, scanning electron microscopy and energy-dispersive X-ray spectroscopy are performed to check the microstructures and compositions of each coating. The nanohardness of the Ni-Co-P, Ni-W-P

and Ni-Mo-P coatings are found to be 1340.32, 633.63, and 1126.224 MPa respectively while Young's modulus are 71.7, 100.75, 105.737 GPa respectively.

Objective III

Thirdly, the objective of the present research work is to assess the corrosion rate of electroless Ni-Co-P alloy coating thereby optimizing and characterizing the coating over the copper substrate. The response parameter, corrosion rate, has been optimized by the variation of parameters like cobalt sulfate, sodium hypophosphite and bath temperature using the Gradient Descent algorithm with root mean square propagation of learning rate. Fifteen coated samples with variable compositions are synthesized as per the three-factor three-level Box-Behnken design (BBD) and their corrosion rates are evaluated from a Potentiodynamic polarization test in aerated 3.5 wt.% NaCl solution. Consequently, the Tafel polarization curve is plotted for the optimized coated sample. A second-order regression model is obtained from the BBD result in Minitab which is used as the input function for the machine learning algorithm in Python. The Analysis of Variance (ANOVA) depicts that the square of cobalt sulfate concentration and the interaction between temperature and cobalt sulfate are the most significant parameters in determining the corrosion rate as per the regression model. The optimum corrosion rate of coated surface suggested by the algorithm is $0.435 \mu\text{m}/\text{Y}$ whereas it is $2.12 \mu\text{m}/\text{Y}$ in the case of the pure copper substrate as found experimentally. The optimum corrosion rate and the corresponding concentration of independent variables obtained from Gradient descent with RMSprop are found to be within a realistic range and in accordance with experimental results.

1.2. Literature Review on FEA and some Advanced Properties of Coating and Thin Films

Electroless coatings have revolutionized the field of coating technology and other thin film protective layers. It is a well-known and widely acknowledged fact that electroless coatings are superior to traditional electrolytic coatings in various aspects. Firstly, it does not take electricity directly during the deposition process increasing the safety in its operation. Furthermore, it can make uniform deposition on various kinds of substrate, especially the non-conducting materials which could not be plated previously by the conventional electrolytic deposition process[1–3]. Besides, it is capable of providing superior mechanical properties like excellent corrosion resistance, hardness, wear resistance, desired level of surface finish etc[4–6]. Several works have been conducted so far to assess these properties and this field is widening day by day in search of more advanced properties like nano-scratch, nano-indentation, fracture behaviour, elastic modulus etc[7–9]. Research in this field is not limited to only simple binary coatings(i.e. Ni-P, Ni-B) but also numerous types of ternary, quaternary and duplex coatings have been synthesized so far in search of better performance as compared to the existing ones[10,11]. It is found that Ni-P/Ni-B duplex coatings are more convenient in use than their single variants[12]. The properties of the simple binary coatings can be further enhanced using advanced heat treatment processes like plasma nitriding as suggested by Tima et al[13]. Similarly, the demand for composite, nano-composite and polymer coatings is increasing gradually as they fulfil the industry needs in a better way. It is found that the incorporation of CeO_2 in the matrix of electroless nickel-boron coating enhances hardness and wear resistance significantly[6]. Recently, the incorporation of carbon nanotubes and graphene as a coating

material has revolutionized this field of research. Both of them have excellent mechanical, thermal and electrical properties which are very suitable to obtain desired surface properties. Wear and friction characteristics of nickel coating are found to be improved as an effect of graphene oxide(GO) in the composite matrix[14]. Besides, electrodeposited GO nanocomposite coating shows excellent tribological properties suitable for a wide range of industrial applications as suggested by Singh et al[15,16]. This research is likely to be continued for a few more decades as the newer and better properties are continuously evolving by combining different alloying elements with the primary electroless nickel coating[17,18].

It is obvious that study and research on the testing of the physical properties of coatings are essential before using them on any engineering equipment. But the study on the design, load analysis and failure criteria of the same is of high importance too when it is used in a practical appliance subjected to external loads. Electroless coating and research related to this field have been done extensively in the past few decades but study on the design and modelling of the coated specimen is not available to that extent. So materials modelling and simulation of the coated sample have the potential to be a crucial area of research in the near future [19]. Engineering design has been the most important part since the advancement of science and technology in the 20th century. A careful engineered solution or design enhances the quality, safety, reliability and cost-effectiveness of a product or service[20–22]. Similarly, when a coating is being applied to a component, it needs to be designed properly based on the load, surface quality requirement and other factors depending on where it is being used. Guo et al[23] conducted a detailed simulation on a space mirror coated with Ni-P and evaluated the stress over the body at an elevated temperature. As the mirror is directly facing the sun, it is highly heated while the surrounding atmosphere is very cold. The analysis was conducted considering this anomaly in the calculation along with the inertia force acting on the mirror assembly. Nowadays finite element analysis is considered to be a very convenient and cost-effective tool to check a component's performance and design feasibility[24,25]. It is capable of providing a realistic result if all the input conditions are accurately given to the compiler. So, without wasting a huge capital and time in doing a series of destructive testing, a good check can also be done through FEA just by knowing the system configuration in detail. Preliminary simulation of complex structures like machinery, bridges, gearbox, valves, engines etc is essential before proceeding with the final design[26–28]. Sometimes the conventional FEA is equipped with augmented reality(AR-FEA) where loads can be applied to the prototype directly[27]. Physical testing of every system is impossible to perform. It can only be done on a small prototype for checking the real-time performance after finalizing all the design parameters and compare it with the software-based results. So, nowadays most of the advanced design proposals require a detailed software-based analysis and FEA is used extensively for this purpose. If only the design of the shaft is considered, huge research has been carried out successfully and still going on based on FEA to investigate the failure criteria, weight optimization, stiffness, fatigue life, fracture behaviour and so on[29–32]. Baranwal et al[8] did a study in Ansys to optimize the difference in induced stress between the layers of Ni-P coating and substrate when it is subjected to internal fluid pressure. Nine different configurations were created by varying thickness of the coating(15, 30, 45 μ m) and internal pressure(50, 100, 150KPa) and finally, the model with minimum stress discontinuity was determined. A similar FEA simulation was conducted by Liu et al[33] to study the thermal stress on a stainless steel substrate coated with Al₂O₃ and Er₂O₃ layers deposited by the physical vapour deposition process.

In this study, a stepped shaft of 110mm in length with varying diameter is taken for modelling and a thin layer of Ni-P coating having a thickness of 50µm is applied over it. In modern applications, a huge number of mechanical systems are used in an environment that is hot and prone to cause a thermal distortion or cracking like boilers, turbines, IC engines, solar collectors etc[28,34–37]. So, design based on thermal loading also becomes a crucial area of research. Taking that issue into consideration, a thermal load is applied to the model by applying a fixed temperature of 200°C on it. Finally, the stress and strain energy induced on the adjacent layers of coating and shaft are compared with each other and their significance is discussed in detail.

1.3. Literature Review on Nano-mechanical Characterization of Coating and Thin Films

Thin films and coating have revolutionized the modern era of science and technology by their unique mechanical and chemical properties. From the small electronic circuit board to the huge aerospace applications, everywhere its presence is dominant. They are capable of providing superior surface properties that cannot be achieved by the bulk substrate material[4,38]. As they are very thin i.e. in the micro to nanometer order, the material requirement is also very less resulting in a very cost-effective surface modification process. Several coating processes have been developed so far like physical vapour deposition, chemical vapour deposition, advanced magnetosputtering, spray coating, electrolytic and electroless coating etc[39–41]. It is to be noted that among the said processes, electroless coating is a very convenient, cost-effective, versatile and easy way of surface plating[39]. Due to their excellent properties like hardness, desired surface roughness, wear, scratch and corrosion resistance and so on, the research and development work in this field has been performed extensively in this field in the past few decades. Nickel-phosphorous(Ni-P) based electroless coating is first suggested by Brenner and Riddle in 1946[42]. After that, tremendous improvement has occurred in this field in search of a better and application-specific surface properties. Basic improvement from the Ni-P coating is the addition of third alloying elements like cobalt, molybdenum, tungsten, carbon fibre, silica etc which are called ternary coating[11,11,17,38,43,44]. Not only that, various types of quaternary, duplex and triplex coatings have been synthesized and characterized so far. In recent times, composite, nano-composite and polymer-based coatings are dominating this research field due to their advanced thermal, chemical, physical and optical properties[6,45–48]. As an example, selective coating on the absorber of the solar thermal energy collector is proven to be highly effective in capturing the solar energy to a larger extent. It allows the incoming solar radiation to have a shorter wavelength while prevents the emission of energy of higher wavelength(infrared). Anti-reflection coating on eyeglasses is also an emerging and broad area of application of coatings. Titanium-nickel plating is found to be very effective to mitigate the corrosion of surfaces by Zhi et al[49] while another study by Ram et al[50] confirms that silicon carbide (SiC) and zirconium oxide(ZrO₂) based nanocomposite coatings are also excellent means to attain anti-corrosive property on the mild steel surface. Besides, surface plating on biomedical implants is an emerging area of research as it allows engineers to invest capital in surface modification only to achieve the desired properties, not on the bulk material[51–54]. Titanium and its alloys coating have been utilized for this purpose due to its excellent biocompatibility and anti-corrosion property in the anatomical environment. Uddin et al[55] have applied physical vapour deposition for plating Titanium nitride on

biomedical devices while a separate study has been carried out by Peng et al where TiCu/TiCuN multilayer coating is deposited by arc ion plating process. There are several other research going on in this field[55,56].

Among the various surface plating processes, electroless coating is a widely accepted method due to its ability to get deposited on a wide range of materials including nonconductive materials. Besides, it is a versatile, easy-to-implement and economic process when used on a mass scale in industries. Several types of surface characterizations of electroless coatings like corrosion, scratch, wear, micro-hardness etc have been studied rigorously but research on the evaluation of important design parameters like nanohardness, Young's modulus, Poisson's ratio, fracture toughness, tensile strength, coefficient of thermal expansion etc has not been possible effectively due to their extremely low thickness value and interference of substrate material while testing any property. Though, recently, a few advanced nanoscale techniques have been suggested by researchers that can evaluate some of the mechanical properties of the coating. As an example, Young's modulus, Poisson's ratio, hardness, creep data and tensile strength can be found by different methods such as nanoindentation, bending test, photoacoustic dispersion, atomic force acoustic microscopy, membrane deflection test etc[57–60]. Besides that, more accurate and refined technologies are being designed day by day. Laser optical measurement is employed by Lee et al to determine the mechanical properties of an aluminium thin film with high accuracy(error<3.5%)[61]. Nanoindentation is the mostly used, convenient and accurate method considered till now for the elastic characterization of thin films. Its indentation depth may be as little as a few nanometers and applied load also can be given in the range of micro to milli Newton. This enables the nanoindenter to evaluate the properties of the outer thin layer of the coating without affecting the substrate material[62–65]. One of the biggest applications of nanoindentation is finding the elastic modulus of thin films which is first calculated reliably by Oliver and Pharr with the help of a nanomechanics based mathematical model[66]. Tsongas et al calculated the elastic modulus of Ni-P and N-P/SiC nanocomposite coating using this method and found the values to be 70 and 114 GPa respectively[64]. A new approach called 'minimum resultant error' is capable of evaluating elastic modulus with very high accuracy with the help of nanoindentation data only. Not only that, this technique can also estimate the values of yield stress, strain hardening exponent and coefficient of the test sample[20]. Apart from the Oliver and Pharr(OP) correlation, a simple mathematical correlation between elastic modulus and hardness of the oxide and nitride thin film has been suggested by Jung et al[67]. Using this correlation, the elastic modulus can easily be approximated by the hardness value of the sample. Besides, it is widely used to find the nanohardness of coatings which is more accurate and reliable as compared to the microhardness value due to very fine indentation depth as discussed earlier. Zhang et al carried out a detailed study on the nanohardness of SiO₂ thin film and concluded that the same is highly dependent on the thickness of the deposited film[68]. Similarly, a rigorous study has been conducted by Ozmetin et al on a 300nm MgB₂ thin film and reported its nanohardness and Young modulus to be around 11.72 GPa and 178.13 GPa respectively using OP correlations[65]. Electroless ternary alloy coatings are also investigated to assess their nanomechanical properties. Ni-W-P coatings are studied using nanoindentation under varying tungsten content and their Young modulus and nanohardness are reported to lie in the range of 150-170 GPa and 5-9 GPa respectively which can be increased significantly when subjected to annealing at 400°C[38]. Electroless Ni-P coating is also investigated by nanoindentation and its average nanohardness and Young modulus are observed to be 7.35 ± 0.26 GPa and 146.46 ± 5.04 GPa which can

further be improved by around 30% by annealing as concluded by Sribalaji et al[69]. Application of nanoindentation in the field of materials research is diverse. It can be successfully utilized to assess the fatigue characteristics of a thin film by providing a cyclic loading with the help of the nanoindenter[70]. Vardanyan et al have performed a study on Nickel bi-crystal using the same technique and found to it to be very effective to estimate the strength of the crystal along grain boundaries having different orientations[71].

In this present study, three different types of widely used ternary coating viz Ni-W-P, Ni-Co-P and Ni-Mo-P are synthesized electrolessly on copper substrates and their nanoscale properties are estimated satisfactorily. All three coated copper substrates are undergone nanoindentation test and their nanohardness and Young's modulus are reported. These properties are very crucial for many advanced designs of critical engineering components subjected to coating on outer surfaces.

1.4 List of Publications in this Field

1. Baranwal RK, Hassan T, Agarwal G, Sarkar S, Majumdar G. Optimization of the stress discontinuity value at the interface of a cylindrical stainless steel substrate and electroless Ni-P coating. Mater Res Express. 2019;6(11). **(Published)**
2. Hassan T, Srivastwa AK, Sarkar S, Majumdar G. Characterization of Plastics and Polymers: A Comprehensive Study. InIOP Conference Series: Materials Science and Engineering 2022 Feb 1 (Vol. 1225, No. 1, p. 012033). IOP Publishing. **(Published)**
3. Hassan T, Sarkar S, Mandal T, Mondal N, Majumdar G. FEA Based Design and Stability Study of Electroless Ni-P Coating Plated over a Stepped Shaft under Thermal Load. Australian Journal of mechanical Engineering, Taylor and Francis. **(Submitted)**
4. Hassan T, Mallick H, Koley I, Sarkar S, Mandal T, Majumdar G. Modelling and Optimization of Corrosion Rate of Ni-Co-P Coating Using Box-Behnken Design and Gradient Descent with RMSprop Algorithm. Engineering Research Express, IOP Publishing. **(Submitted)**

2. Basics of Electroless Coatings

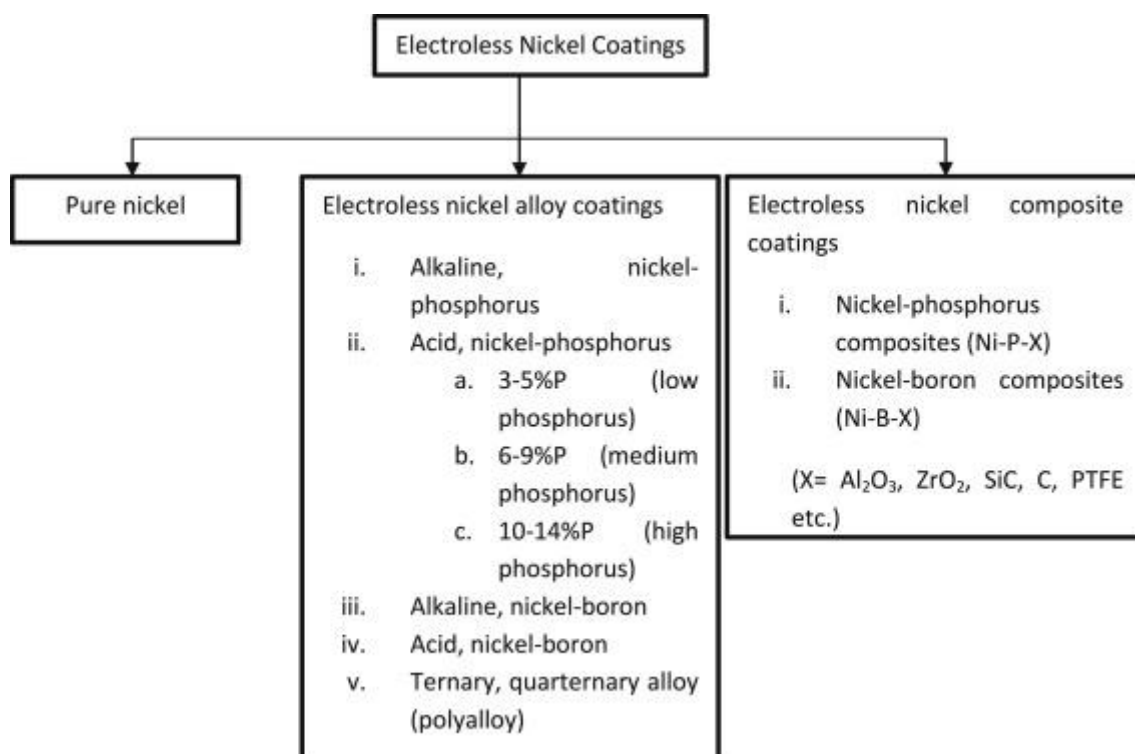
2.1. Introduction to Electroless Nickel Coatings

Electroless coating is nothing but a chemical reduction process which mainly depends on the catalytic reduction of a metallic ion. This entire process occurs in an aqueous solution containing a reducing agent and the subsequent deposition of the metal occurs without the use of electricity. In the past few decades, electroless plating has gained much attention due to its immense capability to produce coatings with excellent hardness, corrosion, wear, abrasion resistance etc. Electroless nickel processes can be classified as Ni-P, Ni-B and pure Ni-based

respectively, depending on the reducing agents used (i.e., hypophosphite, borohydride or dialkyl amino borane and hydrazine) in plating bath. Hypophosphite reduced electroless nickel plating process has gained a huge success because of its low cost, ease of control, and ability to offer good mechanical properties. Although electroless Ni-P deposits give satisfactory performance for several applications, they can be further enhanced by incorporating different alloying elements, composites and nano-particles which have been proven to be highly suitable for crucial applications. Electroless nickel coatings have gained the highest commercial importance among the electroless coating. The desirable properties can be varied to a larger extent by choosing different pH, temperature and bath parameters. In general, electroless plating bath contains a source of metal ions, wetting agents, complexing agents, stabilizers, reducing agents, and buffering agents and its parameters include controlled temperature and pH. Electroless coatings have revolutionized the field of coating technology and other thin film protective layers. It is a well-known and widely acknowledged fact that electroless coatings are superior to traditional electrolytic coatings in various aspects. Firstly, it does not take electricity directly during the deposition process increasing the safety of its operation. Furthermore, it can make uniform deposition on various kinds of substrate, especially the non-conducting materials which could not be plated previously by the conventional electrolytic deposition process[1–3]. Besides, it is capable of providing superior mechanical properties like excellent corrosion resistance, hardness, wear resistance, desired level of surface finish etc[4–6]

2.2. Types of Electroless Coatings

Table 1. Different types of electroless Nickel Coatings



Electroless nickel coatings may consist of four major types are as follows:

- (1) Pure nickel and black nickel coatings
- (2) Electroless nickel alloy coatings
- (3) Electroless composite coatings
- (4) Electroless nanocoatings

Table 1 shows a brief classification of electroless Nickel coating based on its composition.

2.3. Electroless Bath Parameters

Detailed bath parameters for a typical acidic, alkaline and pure Nickel electroless bath are discussed in Table 2 while the detailed functions of different elements in the electroless bath are shown in Table 3.

Table 2. Composition of Pure Nickel, alkaline and acidic electroless bath

SL. No.	Electroless bath	Pure Nickel	Acid nickel-P/B	Alkaline nickel-P/B
1	pH	10.5–11	4.5–5.5 Medium and high P/B; 6.0–6.5 low P/B	8.5–14
2	Temperature (°C)	85–90	75–95	25–95
3	Deposition rate (µm/h)	6–12	10–25	10–15
4	Metal salts or source	Nickel acetate	Nickel sulfate, nickel chloride	Nickel sulfate, nickel Chloride
5	Reducing agents	Hydrazine	Sodium hypophosphite, sodium borohydride, dimethylamine (DMAB)	Sodium hypophosphite, sodium borohydride, dimethylamine (DMAB), hydrazine
6	Complexing agents	EDTA (tetra sodium salt), glycolic acid	Citric, lactic, glycolic, propionic acids, sodium citrate, succinic acid	Citric, lactic, glycolic, propionic acids, sodium citrate, sodium acetate, sodium pyrophosphate
7	Stabilizers	Generally not required	Thiourea, lead acetate, heavy metal salts, organic compounds	Thiourea, lead acetate, heavy metal salts, organic compound, thallium, selenium

8	pH adjusters	Generally not required	Sodium hydroxide, sulfuric acid	Sodium hydroxide, sulfuric acid, ammonium hydroxide
---	---------------------	------------------------	---------------------------------	---

Table 3. Functions of electroless bath parameters

Sl No.	Component/parameter	Function
1	Metal ions	Source of metal
2	Reducing agents	Supply electrons to reduce the metal ions
3	Complexants	Prevent excess free metal ions concentration
4	Accelerators	Accelerate the reducing agent and increase the deposition
5	Stabilizers	Stabilize the bath from decomposition by shielding catalytically active deposition
6	Buffers	Sustain the pH for a long time
7	pH regulators	pH adjustment
8	Temperature	Energy for deposition

2.4. Properties of Electroless Nickel Coatings

2.4.1. Roughness characteristics

Surface roughness is mostly correlated with tribological properties like the coefficient of friction, wear and with some other phenomena like, drags force, stress concentration factor, fatigue life or endurance limit, etc. As electroless nickel coating is a surface modification process, the roughness value of this coating is a crucial factor. A typical application of this coating can be observed in aerospace technology. In most cases, rockets and missiles work in the air and submarine components work in the aquatic atmosphere. Hence to protect them from corrosion a good anti-corrosive coating is needed. The coating should also have low roughness to avoid the huge frictional force with the surrounding environment. In this respect, electroless coating is a good substitute because it gets deposited uniformly over the substrate and follows the surface topography of the same rather than uneven localized deposition. Hence, normally, the roughness of the coating does not deviate much from the roughness of the substrate due to electroless coating. Several researchers have focused on the roughness behaviours of different electroless coatings. Especially in recent years research has increased in the field of composite and nano-coatings. After plating, it has been found that electroless Ni-P and Ni-B coatings exhibit very smooth surfaces[72,73].

2.4.2. Friction & wear characteristics

Since the inception of EN coatings, the properties of such coatings have received huge research attention. Nickel–phosphorus (Ni–P) and Ni–P–X (X–alloying element or nano particles) coatings produced by the electroless technique are extensively used as wear-resistant materials. It has been observed that electroless Ni–P based composite coatings possess better wear resistance than Ni–P alloy coatings[74]. However, due to the complexity of the surface morphology, a wide variety of wear measurement instruments, loading conditions and environment during the wear tests, robust characterization of electroless coatings based on friction and wear is difficult.

The friction and wear behaviour of electroless composite coatings has yet to receive adequate attention from the research community to fully exploit the potential it contains. It is, in general, observed that the friction coefficient of EN coating decreases with an increase in load. The friction study of EN coating concluded that coatings with high phosphorus content have a higher friction coefficient compared to medium or low phosphorus electroless coatings[75]. The friction coefficient was found to be within the range of 0.15–0.35 when tested under the 15 - 60 N loading conditions and the friction coefficient of electroless coatings having 6–7% phosphorous content when tested under low loads was found to be as high as 0.7 [76].

2.4.3. Corrosion characteristics

Electroless coating acts as a protective layer against different types of surface damage like wear, pitting and corrosion. Among the basic Nickel phosphorous coatings, electroless Ni–high P coating exhibits excellent corrosion resistance than electroless Ni–low P and Ni– medium P coatings [77]. Phosphorus can cause the corrosion potential to increase and the corrosion current to decrease. It enhances the anodic and cathodic reactions during the corrosion process, thereby accelerating the anodic dissolution of nickel. The corrosion characteristic of electroless Ni–P coatings is governed by three major factors, namely, the degree of amorphous state, amount of internal stress and the phosphorus percentage. The mutual effect of all of these factors or influence of any one of these factors is responsible for the observed corrosion behaviours. The difference in corrosion resistance between Ni–low P and Ni–high P coatings is particularly due to the difference in structure i.e. non-crystalline, inhomogeneous structure for the low P materials, and an amorphous, homogeneous one for the high P materials.

2.4.4. Microstructure and hardness

In general, the electroless coating is amorphous or microcrystalline in the as-deposited phase but turns crystalline with heat treatment and phosphides and borides are precipitated. The XRD analysis indicates that the as-deposited Ni–P film is a mixture of nanocrystalline and microcrystalline phases. When Ni–P deposits are heat-treated both their crystal structure and microstructure undergo modification. The microcrystalline deposits undergo a crystal growth process and such heat treatment results in a mixture of relatively coarse-grained structures. It was revealed that the coatings contain more than 9% phosphorous leading to a micro nanocrystalline structure. Upon heat treatment at 400°C, Ni–P deposits produce Ni₅P₂, Ni₂P and NiP₂ as major compound constituents [78]. Incorporations and co-depositions may modify the structure to a great extent that may contribute to the enhanced properties in the coating.

Among the various metallization processes, electroless metal plating is a preferred way to produce metal-coated fabrics due to the attractive advantages such as uniformity of coverage, excellent conductivity, the possibility of metalizing non-conductors and flexibility. Ni–P

plating is applied in order to render abrasion resistance to electromagnetic shielding fabrics [79]. The advantages of modifying the properties of electroless nickel coatings by suitable surface treatments and the incorporation of various elements (copper, tungsten, etc.) and particles (SiC, TiO₂, Si₃N₄, etc.) have been utilized by various researchers to evaluate the suitability of these coatings for various applications. By observing the expansion possibilities of electroless nickel coatings, more advanced tribological application of the coatings may be expected.

3. Finite Element Analysis

3.1. Brief Discussion on FEA

The Finite Element Analysis (FEA) is the simulation of any given physical phenomenon using the numerical technique called the Finite Element Method (FEM). It is applied to obtain an approximate solution to boundary value problems often called field problems. Field variables are the dependent parameters and get evaluated by the field structure and boundary constraints. Engineers use FEA software to reduce the number of physical prototypes and experiments and optimize components in their design phase to develop better products and faster results while saving on expenses. It is necessary to use mathematics to comprehensively visualize and quantify any physical phenomena such as statics and dynamics problems, fluid mechanics, thermal loading and transport, wave propagation, growth of biological cells, etc. Most of these processes are described using Partial Differential Equations (PDEs). However, for a computer to solve these PDEs, numerical techniques have been developed over the last few decades and one of the prominent ones, today, is the Finite Element Analysis. Differential equations not only describe natural phenomena but also physical phenomena encountered in engineering mechanics. These partial differential equations (PDEs) are complicated equations that need to be solved in order to compute relevant quantities of a structure like stresses (σ), strains (ϵ), etc. in order to estimate the structural behaviour under a given load. It is important to know that FEA only gives an approximate solution to the problem and is a numerical approach to getting the real result of these partial differential equations. Simplified, FEA is a numerical method used for the prediction of how a part or assembly behaves under given conditions. It is used as the basis for modern simulation software and helps engineers to find weak spots, areas of tension, critical zones etc. in their designs. The results of a simulation problem solved by the FEA method are usually depicted via a colour scale that shows, for example, the pressure distribution over the object.

Example: Spring-Force System as Finite Element

A linear elastic spring is a mechanical device capable of supporting axial loading only, and the elongation or contraction of the spring can be approximated to be directly proportional to the applied axial load. It is the simplest and most convenient example to understand how FEA works. The constant of proportionality between deformation and load is referred to as the spring constant, spring rate, or spring stiffness k , and has units of force per unit length. As an elastic spring supports axial loading only, we select an element coordinate system (also known as a local coordinate system) as an x-axis oriented along the length of the spring, as shown.

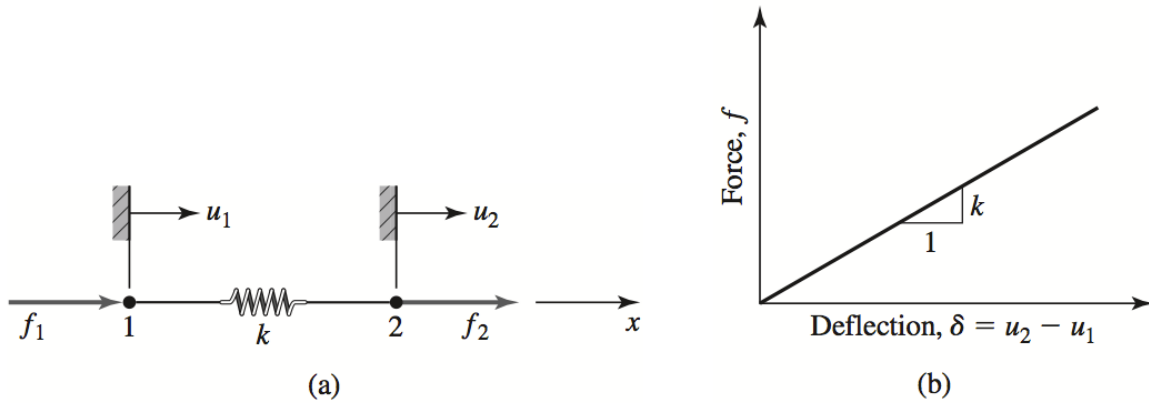


Fig. 1(a). Linear spring element with nodes(1, 2), nodal forces(f_1, f_2) and displacements(u_1, u_2)

Fig. 1(b). Linear load-displacement curve of the spring.

Assuming that both the nodal displacements are zero when the spring is undeformed, the net spring deformation is given by:

$$\delta = u_2 - u_1$$

and the resultant axial force in the spring is:

$$f = k\delta = k(u_2 - u_1)$$

For equilibrium,

$$f_1 + f_2 = 0 \text{ or } f_1 = -f_2,$$

Then, in terms of the applied nodal forces as:

$$f_1 = -k(u_2 - u_1)$$

$$f_2 = k(u_2 - u_1)$$

which can be expressed in the matrix in the following form:

$$\begin{bmatrix} k & -k \\ -k & k \end{bmatrix} \begin{Bmatrix} u_1 \\ u_2 \end{Bmatrix} = \begin{Bmatrix} f_1 \\ f_2 \end{Bmatrix}$$

$$\text{Or, } [k_e]\{u\} = \{f\}$$

where, $[k_e] = \begin{bmatrix} k & -k \\ -k & k \end{bmatrix}$ and called elemental stiffness matrix. It is an essential task to define the stiffness matrix first to solve any FEA problem and performed it by the different software packages available in the market. We just need to define the model or the field where the solution is to be performed with necessary boundary conditions. Besides, the physical properties of the model are needed as per the solution requirement. $\{u\}$ is the column vector of nodal displacement and $\{f\}$ is the column vector(matrix) of nodal forces.

Diagram for two spring systems:

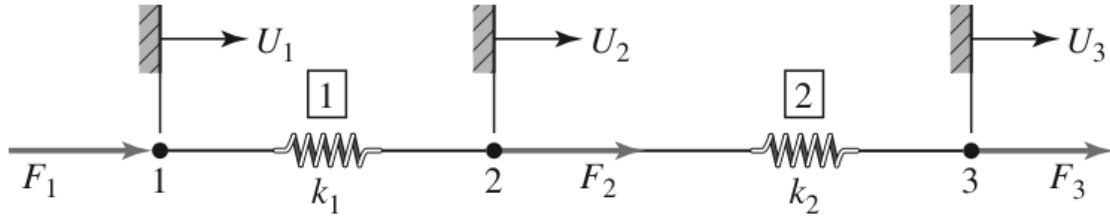


Fig. 2a. Three node system with external forces F_1 , F_2 and F_3

Free body diagram:

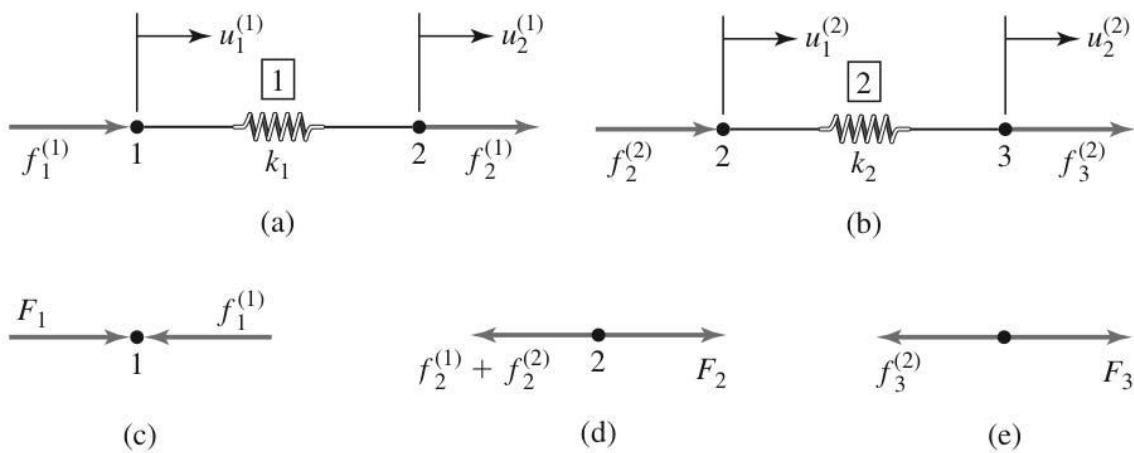


Fig. 2b. FBD of the system with internal nodal forces f_1 , f_2 and f_3

3.2. Application of FEA on Coating-Substrate Assembly

The application of finite elements in the field of engineering is widespread as it is capable of providing a realistic solution to a model under given boundary conditions. Engineering designers especially, apply FEA extensively to assess the approximate result of a proposed designed product when subjected to various loading conditions. It is a very efficient, cost-effective and fast decision-making process in a non-destructive manner. Nowadays coatings and thin films are used in almost every engineering industries to ensure desired surface properties which cannot be obtained from the bulk parent material. Now, if the coating is applied on equipment, it is very crucial to perform the design and stability analysis of the same along with the bulk. Performing practical testing on the manometer and micro meter order coatings might be impossible or very costly so, FEA here becomes a very useful tool to analyze and simulate thin films under practical loading conditions. It will help the designer to assess whether the coating is suitable under the given design conditions or if a modification in the coating's characteristics is needed. Some potential industries where the use of coatings is done extensively are aerospace, automobile, food processing, high-capacity pressure vessels, shipbuilding etc. In this thesis work, one separate study is performed using FEA simulation and the results of the same are discussed in detail. It is to be noted that the results are quite

interesting and match with the general design principles. The following sections discuss those concepts in detail.

3.3. FEA Based Design and Stability Study of Electroless Ni-P Coated Stepped Shaft under Thermal Load

3.3.1. Substrate Preparation and Coating Deposition

Copper substrate of the size of $15 \times 6 \times 0.3 \text{ mm}^3$ which is cut from the bigger copper foil (99.0% pure, Lobachemie) for the deposition of electroless nickel coatings. After the selection of substrate, it is then subjected to cleaning process in dilute HCl solution to get rid of foreign particles and corrosion products followed by rinsing in deionized water. Before starting coating deposition, it is dipped into palladium chloride solution (55°C) to activate the substrate surface by overcoming the initial energy barrier and start the deposition process rapidly as soon as the substrates are dipped in the electroless bath. This also incorporates a significant amount of deposit thickness, higher deposition rates, and good adhesion of the coatings to the substrate.

Table 4. Bath Composition for Ni-P coating over copper substrates

Bath composition	Quantity
Nickel Sulphate ($\text{NiSO}_4 \cdot 6\text{H}_2\text{O}$)	30g/L
Sodium Hypophosphite ($\text{NaH}_2\text{PO}_2 \cdot \text{H}_2\text{O}$)	20 g/L
Tri-sodium Citrate Dihydrate ($\text{Na}_3\text{C}_6\text{H}_5\text{O}_7 \cdot 2\text{H}_2\text{O}$)	15g/L
Sodium Acetate (CH_3COONa)	5 g/L
Time	80 minutes
Bath volume	250 ml
Bath Temperature $^\circ\text{C}$	85 $^\circ\text{C}$

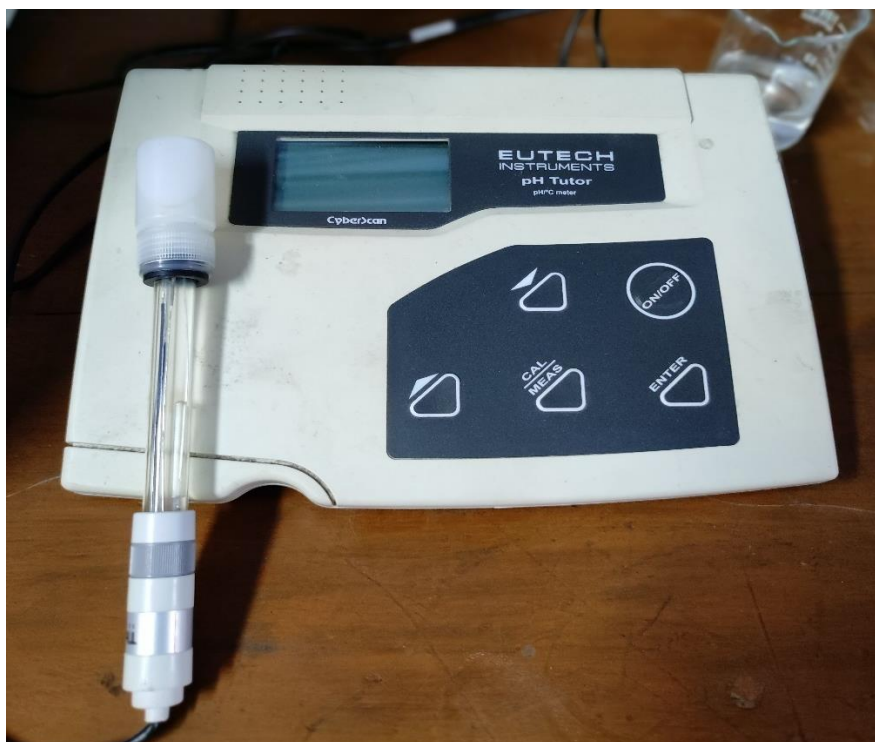


Fig. 3. pH meter used for monitoring the pH of electroless bath



Fig. 4. Electroless bath preparation having a bath volume of 250 mL

Nickel Sulphate is used as the source of nickel with sodium hypophosphite which is the reducing agent and sodium citrate is added as a complexing agent. Sodium acetate used in the bath works as a buffering agent and stabilizes the pH of the solution. The pH of the solution is maintained at around 5 by continuous monitoring with a pH meter (as shown in Fig. 3) and the temperature of the bath is maintained at 85°C by an automated heating system. Details of the

bath parameters are provided in Table 4. Four copper substrates are dipped into the electroless bath having a volume of 250 ml and deposition is carried out for a period of 80 minutes. After that, the substrates coated with Ni-P are taken out of the bath and rinsed in distilled water. Now the coated sample is dried and mounted with help of epoxy resin. It is done with utmost caution as the sample is very thin(0.3mm). Special care is also provided to assure proper adhesion of the sample to the mounting material.

3.3.2. Modelling and Details of FEA

3.3.2.1. Modelling of Shaft-Coating Assembly

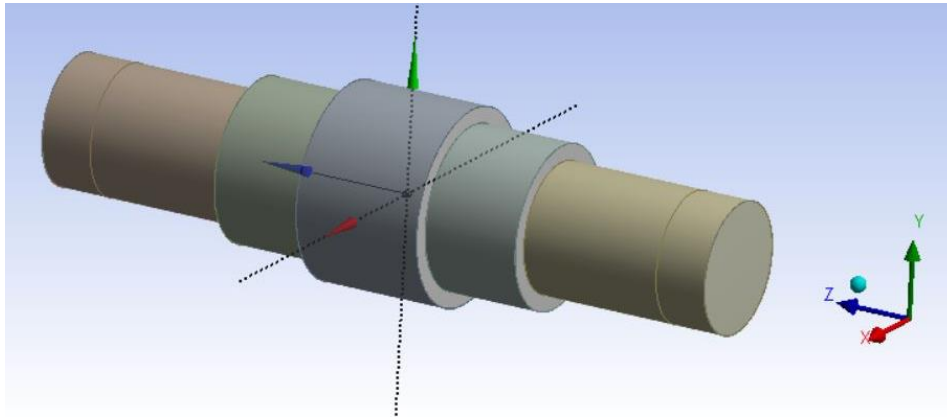


Fig. 5. Global coordinate system G_{xyz} (cartesian)

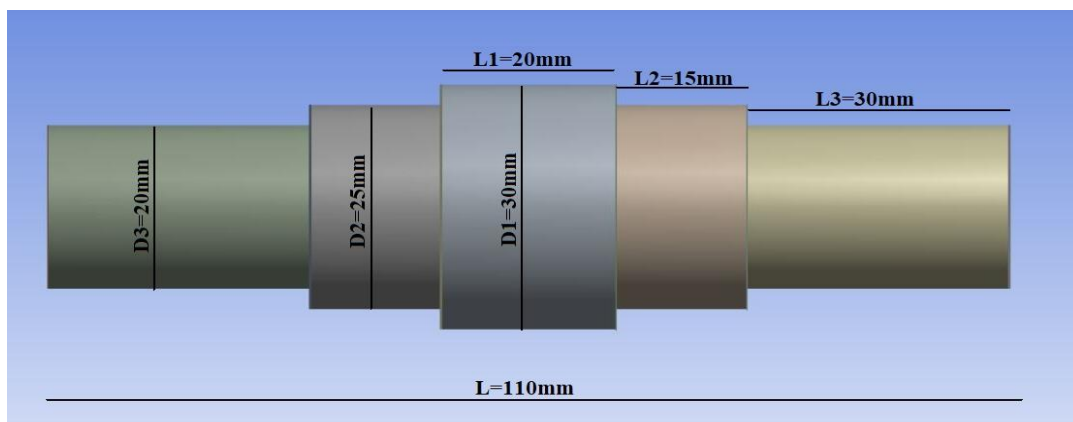


Fig. 6. Dimension of the shaft(substrate) before applying coating on it

Present analysis is done in Ansys workbench where a series of simulations are possible with different types of systems and input conditions. The static structural tab is selected for performing thermal analysis on a shaft as the thermal loading given by a fixed temperature resembles a static loading. All the points are defined with respect to the global coordinate system which is fixed on the mid-span of the shaft as shown in Fig. 5. The shaft is modelled in three axisymmetric segments having diameters of 30, 25 and 20 mm respectively as shown in Fig. 6.

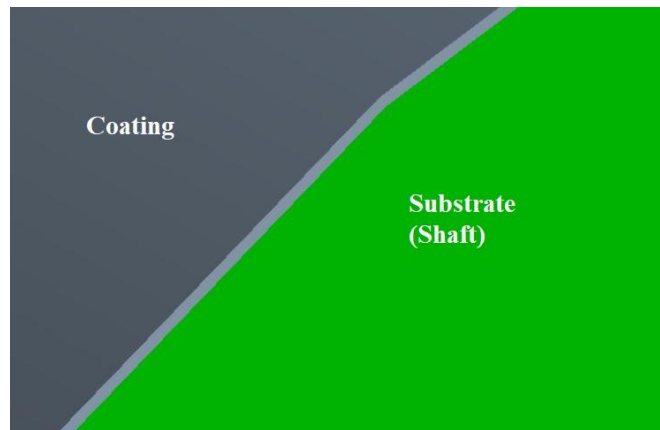


Fig. 7. Coating of 50 μ m is applied on the shaft body

Total length of the shaft is 110mm before applying the coating and it becomes 110.1mm when Ni-P coating of 50 μ m thickness is applied over the entire body(Fig. 7). Similarly, the respective diameters shown in Fig. 2 increase by 0.1mm each as the increase in diameter becomes $50\mu\text{m} \times 2 = 100\mu\text{m}$ or 0.1mm. After that, two separate bodies are generated in the simulation model and they are assigned the respective material properties.

3.3.2.2. Input details for the Simulation

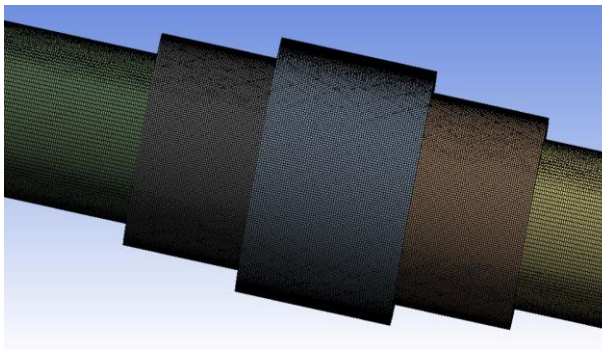


Fig. 8. Meshed structure of the coating-shaft assembly

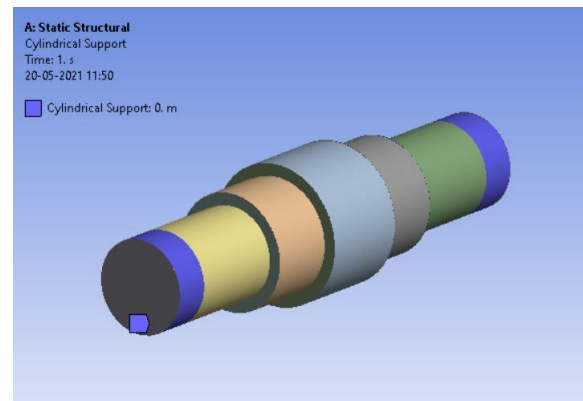


Fig. 9. Cylindrical supports on the two ends of the shaft

It is the preliminary and most essential task to determine the material properties of the model being analyzed in Ansys. For performing this present simulation the necessary data are elastic modulus, Poisson's ratio and coefficient of thermal expansion which are to be inserted in the engineering data section before initiating the evaluation. After completing the modelling part in the Design modeller, a series of settings are performed for enabling the coating-shaft assembly to be solved by FEA. Firstly a bonded connection is created at the contact layer of the coating and shaft. Consequently, a mesh of size 3 mm is generated in the shaft body while a default soft mesh is applied to the Ni-P coating(Fig. 8). It is to be noted that mesh size is kept on the moderate side to minimize the computation time as the prime objective here is to study the nature of the result. Evaluation of thermal stress or strain energy will require a constraint

on the body as a fully free body will not generate any stress. So, cylindrical supports at the two ends of the shaft are applied to give it a bearing-like character(Fig. 9). Axial and radial components of the cylindrical supports are made fixed while the tangential component is kept free by manual setting.

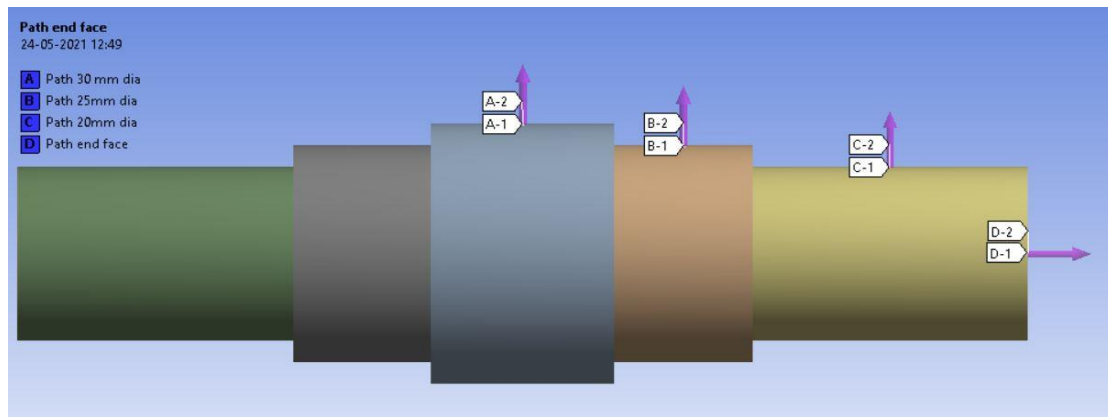


Fig. 10. Location of paths A, B, C, D created in the model

Table 5. Geometrical details of the paths(Coordinates are defined with respect to G_{xyz})

Path name	Start coordinate(mm)	End Coordinate (mm)	Length(μm)
A	(0, 14.95, 0)	(0, 15.05, 0)	100
B	(0, 12.45, 17.5)	(0, 12.55, 17.5)	100
C	(0, 9.95, 40)	(0, 10.05, 40)	100
D	(0, 0, 54.95)	(0, 0, 55.05)	100

Finally, the load is applied to the bodies in the form of temperature. Thermal stress, total deformation, thermal strain and strain energy are evaluated all over the bodies. Besides, a separate investigation is done to check the variation of strain energy and thermal stress between the two adjacent bodies viz Ni-P coating and stainless steel shaft. This is an important area of this research work for which four separate straight line paths are created on the model. Each of them starts from the shaft body and passes through the 50 μm coating radially outwards as shown in Fig. 10. The start and end coordinates of the paths are shown in Table 5. Paths are created in such a way that they can cover the interfacial zone of coating and substrate enabling us to do a comparative study between the same. Paths A, B and C are set in three different zones having different diameters while D is set at the end face of the shaft so that the effect of the thermal loading at different zones can be comparatively studied.

3.3.3. Characterization of Electroless Ni-P Coating

Elastic Characterization

Evaluation of mechanical properties of thin films, coatings and protective layers have always been a challenging issue for researchers as unlike the traditional metals and composites, they are not readily available in a regular shape that can be conveniently tested. The coatings comes always with the base metal or substrate so testing the coating separately is not an easy task. Though, in today’s scenario, few advanced nanoscale techniques can evaluate some of the mechanical properties of the coating. As an example, Young’s modulus, Poisson’s ratio, hardness, creep data and tensile strength can be found by different methods such as nanoindentation, bending test, photoacoustic dispersion, atomic force acoustic microscopy, membrane deflection test etc[12,57,80–83]. Besides that, more accurate and refined technologies are being designed day by day. Laser optical measurement is employed by Lee et al to determine the mechanical properties of an aluminium thin film with high accuracy(error<3.5%)[7].

$$E = 2G \times (1 + \mu) \quad (1)$$

$$E = 3K \times (1 - 2\mu) \quad (2)$$

Table 6. Material properties of coating and shaft[8,23,84].

Material	Young’s Modulus (GPa)	Poisson’s Ratio (GPa)	Rigidity Modulus (GPa)	Bulk Modulus (GPa)	Coefficient of thermal expansion (CTE) (K^{-1})
Ni-P coating	55.5	0.24	22.38	35.58	13×10^{-6}
Stainless steel shaft	193	0.31	73.66	169.3	17×10^{-6}

Recently, a new method named ‘minimum resultant error’ has been employed to evaluate some complex mechanical properties of titanium nitride thin film like strain hardening exponent, strain hardening coefficient and yield stress[20]. For this present study Young’s modulus is determined from the load-displacement data of the nanoindentation test which is nowadays considered to be one of the most efficient and fastest mechanical characterization processes for coatings and thin films. The required models to determine the parameter are taken from published literature[63,85,86]. An average value of Poisson’s ratio is considered based on published works as shown in Table 6. Rigidity and bulk modulus are obtained from these two data using the formulae for isotropic elasticity(Equation 1, 2).

Microstructural Characterization

Table 7. Elemental composition of the Ni-P coating

Element	Weight %	Atomic %
Ni	12.47	21.26
P	87.53	78.74

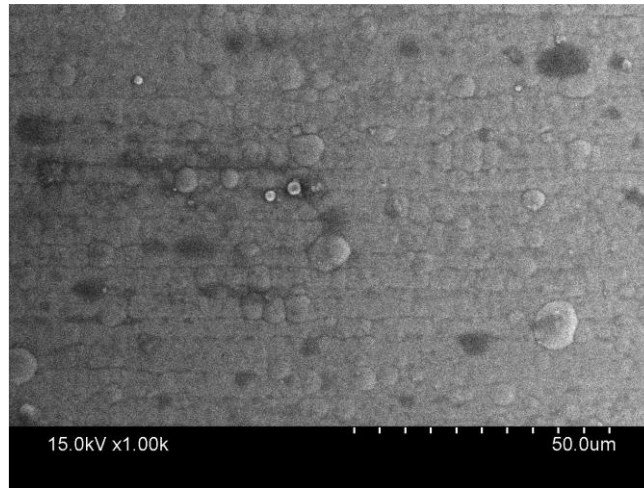


Fig. 11a. SEM image of as-deposited Ni-P coating

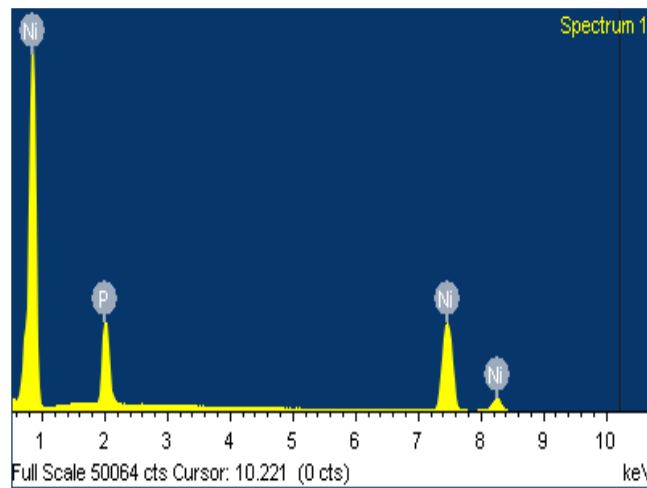


Fig. 11b. EDAX spectra of the Ni-P coating

The physical properties of Ni-P coating are highly dependent on its composition, nature and uniformity of the deposition. So while using some data, its basic compositions need to be specified. The SEM and Energy Dispersive X-ray analysis (EDAX) spectra of the sample used for the nanoindentation test are shown in Fig. 11a and 11b respectively. Under SEM the characteristics of the electroless deposit have been revealed. Close deposition of round globular particles is exposed distinctly though, size variations from 2– 5 μm are common. Fig. 11a shows no presence of cracks and holes on the surface of the coatings which suggests a highly compact coating with a minimum defect is formed. From the EDAX analysis, the percentage composition of the coated deposits has been revealed as shown in Table 7. The amount of phosphorus present in the coatings obtained from the EDAX test reveals that it is a high phosphorus coating.

Thermal Characterization

Like the many physical properties discussed here, thermal properties i.e. heat capacity, thermal conductivity, coefficient of thermal expansion (CTE) etc are essential for the analysis of thin films under thermal loading. Research in this field is still going on to evaluate these properties

reliably with minimum error. No absolute measurement method is available till now but the recently published techniques like thin-film calorimeter, laser flash method and pulsed photothermal radiometry are capable of providing the data with finer accuracy[87–90]. The specific thermal property required for the present analysis is the CTE. Evaluation methods of CTE of Ni-P coating are suggested by a few researchers. The methods include push rod dilatometer[84], strain gauge technique[91], image processing[92] and so on. The same can also be evaluated by considering the contribution of each constituent of the coating in thermal expansion. This modelling will require the percentage of different components present in equilibrium condition and their individual CTEs[80]. Literature review suggests that the CTE of Ni-P varies significantly with the compositional change and operating temperature. So, it is not possible to get a unique value of the CTE. For our study, an averaged data is taken measured based on dilatometry as suggested by Kinast et al[84] while it is to be noted that the data required for the stainless steel are taken from the default Ansys catalogue. The input data of the shaft and the coating are shown in Table 6.

3.3.4. Result and Discussion

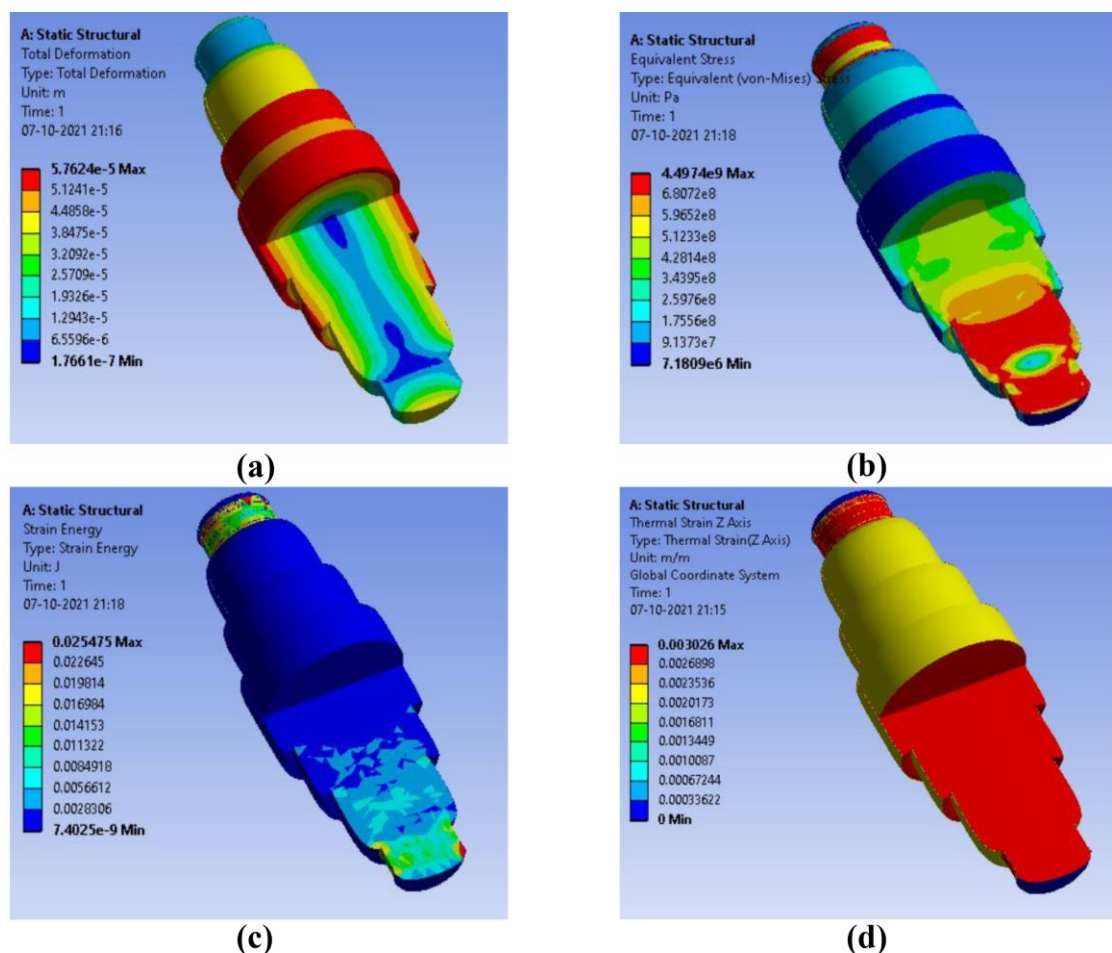


Fig. 12. (a) the total deformation, (b) equivalent stress, (c) strain energy and (d) thermal strain generated in the assembly of shaft and coating

$$\text{Thermal strain } (\epsilon_t) = \alpha \times \Delta t \quad (3)$$

where α is the linear CTE and Δt is the temperature change.

$$\text{Equivalent stress } (\sigma_e) = \sqrt{\frac{(\sigma_1 - \sigma_2)^2 + (\sigma_2 - \sigma_3)^2 + (\sigma_3 - \sigma_1)^2}{2}} \quad (4)$$

Where σ_1 , σ_2 and σ_3 are the principal stresses in the element. σ_e is a good measure of the state of stress in material as it considers the effect of all three stress components.

$$\text{Strain energy per unit volume} = \frac{1}{2} \times \text{stress} \times \text{strain} \quad (5)$$

The main objective of this simulation is to investigate the real-life occurrence in the coating-substrate assembly in an easier and cost-effective way. As the system is subjected to thermal loading, the thermal strain (Equation 3) and deformation become important design parameters. The basic data required for evaluating these values is the coefficient of thermal expansion (CTE) as discussed earlier. Besides, equivalent stress (Equation 4) and strain energy (Equation 5) are calculated which are essential for studying the failure criteria and the level of stability of the model at that particular temperature. Value of total deformation, equivalent stress, strain energy and thermal strain evaluated all over the body are represented in the colourmap as shown in Fig. 12a, b, c and d respectively.

3.3.4.1. FEA Result on the Entire Assembly

From Fig. 12a it is evident that the total deformation is least in the end zones of the shaft while the mid-outer zone experiences the largest deformation. This is simply because the end sides of the shaft are subjected to cylindrical support resulting in a constrained deformation while the mid zone is least constrained as it is farthest from the support. For a similar reason, the highest equivalent stress is generated on the end sides and the lowest on the mid-span of the shaft as shown in Fig. 12b. In the case of strain energy, the value is higher on the support zones as the stress induced in those areas is higher and it is dominating the effect of strain. For this reason, the strain energy value is higher in spite of the lower value of total deformation in the support zones (Fig. 12c). An important observation can be made from Fig. 12d that the thermal strain generated is lower in the coating as compared to the shaft as the CTE value used for Ansys simulation is lower for the former as compared to the latter (refer to Table 6). This may cause the generation of residual stress in the interface of coating and shaft making the outer layer more vulnerable to failure. So designers should try to minimize the difference between CTEs of coating and substrate especially when the system is exposed to a hot environment.

3.3.4.2. Results Obtained along the Paths

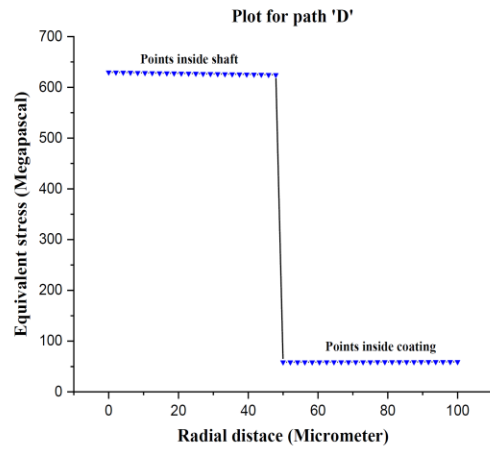
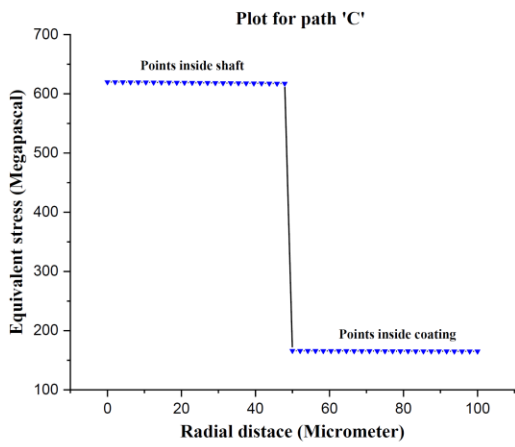
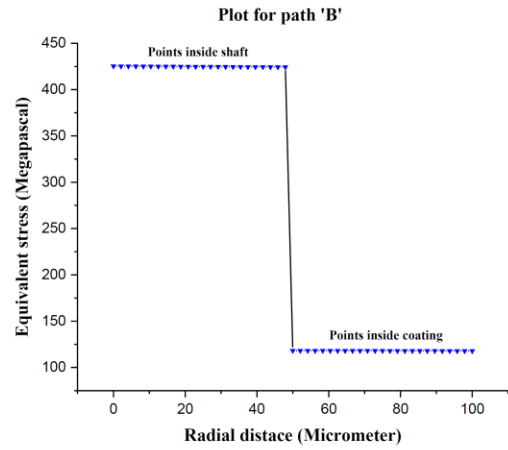
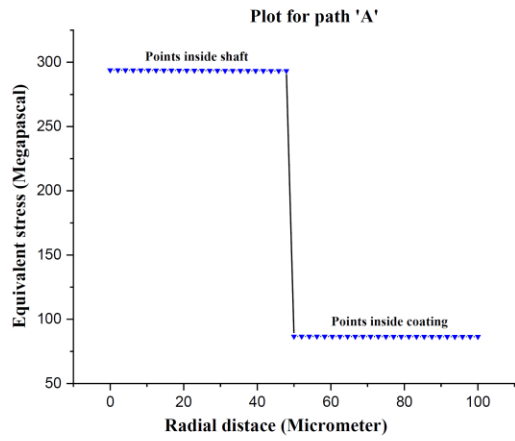


Fig. 13. Variation of equivalent stress along the paths A, B, C and D respectively.

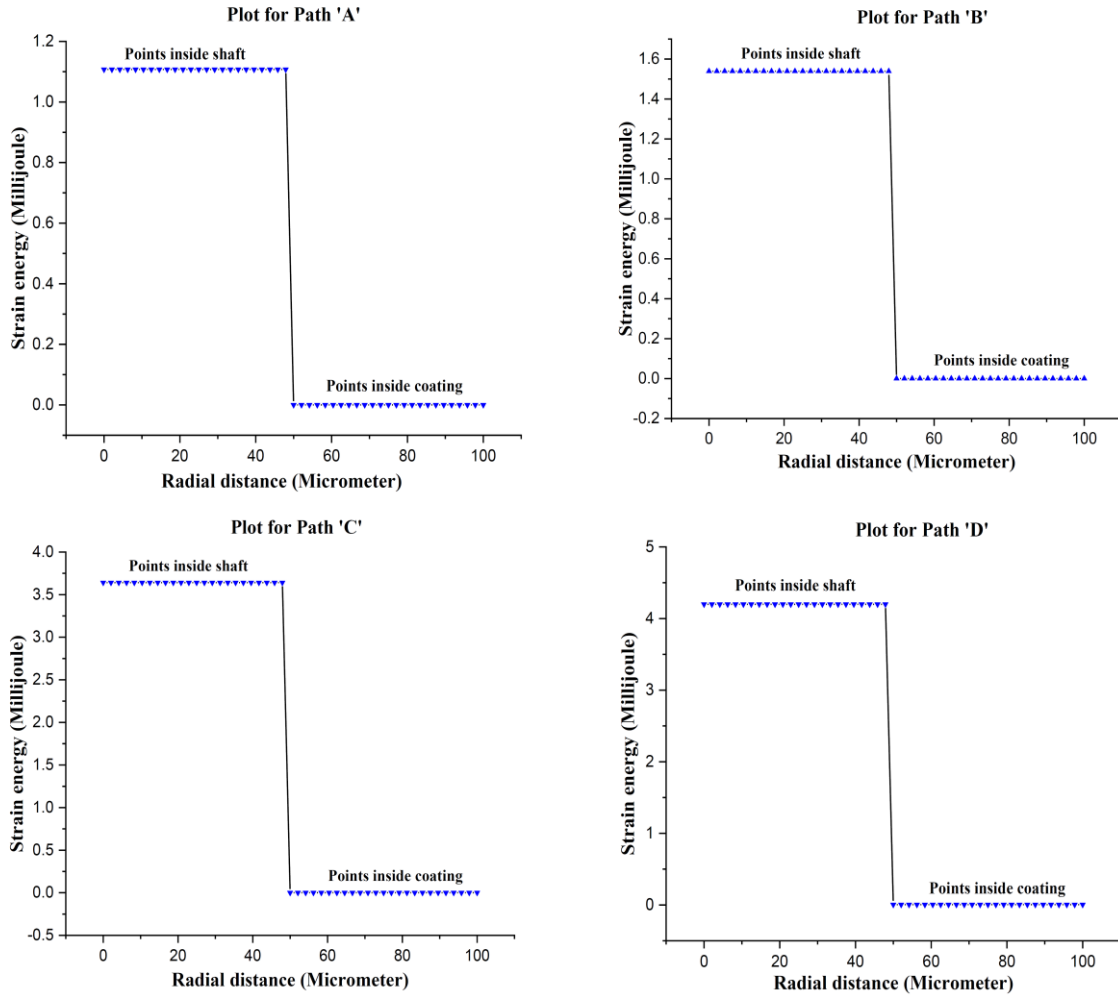


Fig. 14. Variation of strain energy along the paths A, B, C and D respectively

A separate study is performed to analyze results along a straight line in the model which is a very helpful tool to check the variation of data along that line. The value of equivalent stress (σ_e) and strain energy (SE) are evaluated along the four different paths as discussed earlier and the data are plotted against the radial distance with respect to the axis of the shaft as shown in Fig. 13 and 14 respectively. The prime objective of finding the data along a path is to calculate the change in the values of σ_e and SE between the coating and the shaft. This change may be a helpful measure to predict the design stability of the coating over the surface of the substrate. From the atomic scale to a macro scale substance, everything is connected to energy in various ways. It is also an important scientific fact that the energy level is indirectly proportional to the level of stability. So every object in this universe is trying to minimize its energy to gain better stability, like the electron on the outer orbit in an atom is very unstable and mainly responsible for chemical bonding because of its higher energy state while the reverse happens to the inner orbit electron due to lower energy level [93–95]. In the case of elastic material, strain energy is one form of potential energy which is generated in a deformed body due to the generation of stress. The body which has higher SE or induced stress is capable of performing higher elastic work making itself less stable and more prone to cause failure. Han et al[96] used the advanced concept of strain and resonance energy to analyze the stability and performance of explosives.

Similarly, the ligand strain energy of the metal-organic framework (MOF) is compared with its stability by Shustova et al[97]. The main objective here is to justify that the strain energy is an important determining parameter for the design stability of an elastic body.

Table 8. Variation of parameters between adjacent layers of Ni-P coating and the shaft.

Parameters	Discontinuity in path A	Discontinuity in path B	Discontinuity in path C	Discontinuity in path D
Equivalent stress (σ_e) (MPa)	207	306	451	566
Strain energy (SE) (Millijoule)	1.11	1.54	3.64	4.19

From Fig. 13 and 14, it is visible that there is a sharp discontinuity in the values of σ_e and SE between the two contacting layers of coating and shaft at every location. This occurs mainly due to the variation in the mechanical properties and changes in the nature of bonding. A bonded(fixed) contact is applied between the coating and shaft in Ansys, as the electroless coatings are firmly bonded with the substrate by adhesion and molecular diffusion. It is also observed that the value of discontinuity varies significantly at different locations of the shaft. It is lowest for path ‘A’ and increases gradually up to path ‘D’ as shown in Table 8. This is a very crucial observation that can be directly correlated with the stability of the model. As discussed earlier that the shaft is subjected to cylindrical support at the ends which causes a heavy stress concentration due to the constrained nature of the support. It makes these zones very unstable and most vulnerable to failure and crack propagation in case it is a brittle material. This instability can be interpreted by the highest value of stress and SE discontinuity in path ‘D’ (Fig. 13, 14). The induced stress decreases gradually as the distance from the support increases making the mid-position of the shaft least stressed and most stable. The same can also be validated by the decreasing discontinuity value of SE and σ_e from path D to A which is located at the mid-span of the shaft(refer to Table 8). So, simply it can be said that the higher difference in those values between the coating and substrate layers reduces the stability of the bond, may cause premature separation of the coating from the substrate and adversely affect the scratch, wear and corrosion resistance of the electrolessly plated surface. The same is also concluded by Baranwal et al[8] from their FEA study on a pressure vessel.

4. Nano-Mechanical Characterization of Electroless Ni-Co-P, Ni-W-P and Ni-Mo-P Alloy Coatings: A Comparative Study

4.1. Sample Preparation

A copper sheet of 0.508mm thickness is cut into small squares of size 10×10mm². The samples are then flattened by suitable arrangement followed by polishing with the help of emery paper having grit size 500, 1000 and 1500 respectively. Next, the samples are degreased and cleaned in dilute HCl solution and rinsed in distilled water properly. Before dipping the samples in the electroless bath, the samples are activated in palladium chloride solution (DI water + HCl + PdCl₂) heated at 55°C. This ensures a significant amount of deposit thickness, higher deposition rates and good adhesion of the coatings to the substrate. The volume of DI water in the electroless bath is taken 250ml and four copper samples are dipped for a single run as shown in Fig 15. The samples are hung from a glass holder placed on the beaker with the help of thin copper wires.



Fig 15. Electroless bath with the copper substrate placed over the heating plate

Table 9. Electroless bath compositions for the synthesis of Ni-Co-P coating

Name of the Material	Concentration
Sodium Hypophosphite	30 g/L
Nickel Sulphate	25g/L
Cobalt Sulphate	15g/L
Ammonium Sulphate	10g/L
TCD	15g/L
Sodium Acetate	5g/L
Deposition Time	80 Minutes
Bath Volume	250ml
PH	5.5-6

Table 10. Electroless bath compositions for the synthesis of Ni-W-P coating

Name of the Material	Concentration
Sodium Hypophosphite	25 g/L
Nickel Sulphate	35g/L
Sodium Tungsten Dihydrate	20g/L
TCD	32g/L
Sodium Acetate	4g/L
Deposition Time	80 Minutes
Bath Volume	250ml
PH	8

Table 11. Electroless bath compositions for the synthesis of Ni-Mo-P coating

Name of the Material	Concentration
NiSO ₄ ·6H ₂ O	30 g/L
NaH ₂ PO ₂ ·H ₂ O	20 g/L
Na ₃ C ₆ H ₅ O ₇ ·2H ₂ O	30 g/L
Na ₂ MoO ₄ ·2H ₂ O	5 g/L
lactic acid	10 g/L
Sodium dodecyl sulphate	0.08 g/L
Pb(CH ₃ COO) ₂ ·3H ₂ O	0.02 g/L
Bath Volume	250ml
PH	8.4

Nickel Sulphate is used as the source of nickel with sodium hypophosphite which is the reducing agent and sodium citrate is added as a complexing agent. Sodium acetate used in the bath works as a buffering agent and stabilizes the pH of the solution. The pH of the solution is maintained by continuous monitoring by a pH meter and the temperature of the bath is maintained at 85°C by an automated heating system. Details of the bath parameters for Ni-Co-P, Ni-W-P and Ni-Mo-P are provided in Tables 9, 10 and 11 respectively. Deposition is carried out for a period of 80 minutes and then, the coated substrates are taken out of the bath and rinsed in distilled water. Now the coated samples are dried and preserved in an air tight container.

4.2. Nanoindentation test on the Coated samples

Test is carried out using a high precision Anton Paar GmbH Nanoindenter® (model LV-700) having a sharp Berkovich indenter under a maximum load of 10mN with a loading and unloading rate of 20mN/min. Too small load may affect the accuracy of the result so the load is chosen in such a way that the result becomes accurate and the penetration depth do not cross the coating thickness. It is a standard convention that the depth of penetration should lie within 10% of the coating thickness so that the interference of the substrate material can be eliminated[62,65]. In our case, the coating thickness is 10-20µm while the maximum depth in the indentation test is in the range of 300-700nm which is satisfying the condition. Details of the nanoindentation testing method is provided in Table 12. Determination of mechanical properties is still very challenging as it is highly dependent on the uniformity of the deposit and the process parameters of the electroless deposition. To enhance the accuracy of the result,

nanoindentation is performed on five distinct positions of each sample and finally, the average value is calculated.

Table 12. Details of the nanoindentation test and loading conditions

Maximum load	10mN
Loading rate	20 mN/min
Unloading rate	20 mN/min
Holding time at peak load	10 sec
Acquisition rate	10 Hz
Approach distance	2000 nm
Approach and retract speed	2000 nm/min
Stiffness threshold	500 $\mu\text{N}/\mu\text{m}$

4.3. Mathematical Model Used for the Evaluation of Nanomechanical Properties

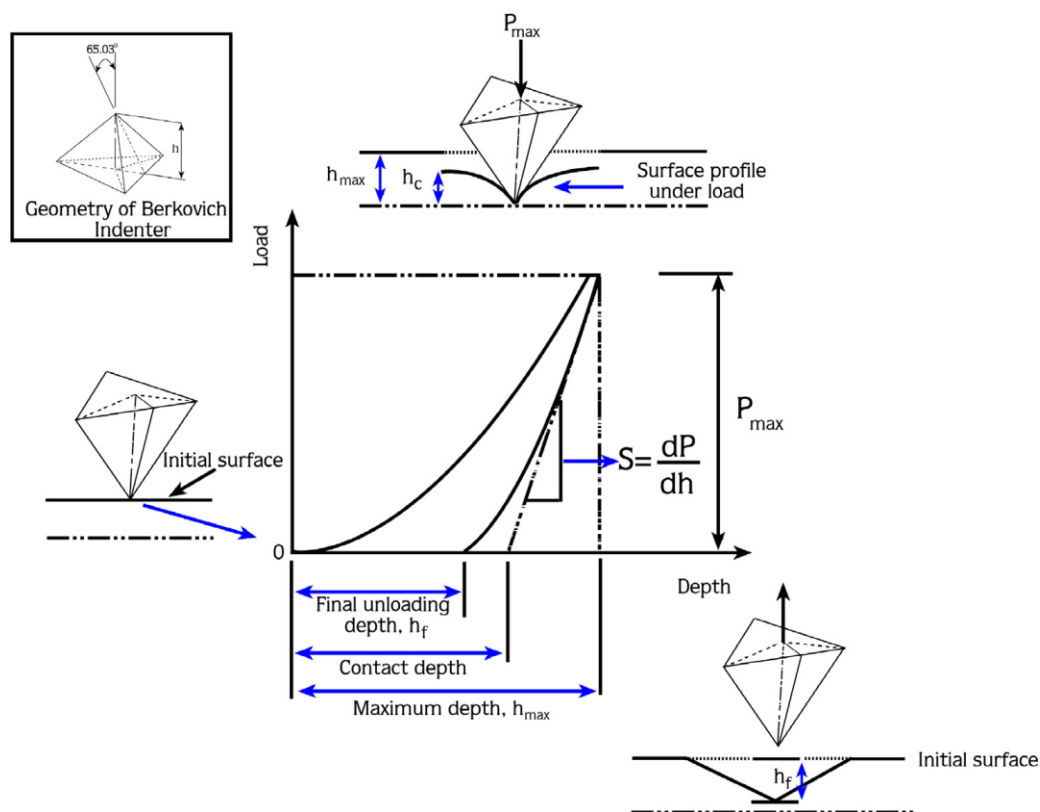


Fig 16. Representation of different parameters for the analysis of the nanoindentation results.

In the Oliver Pharr[66] analysis, nanohardness(H_N) and elastic modulus(E) are determined from the load–depth curve of nanoindentation. The curve generated by the nanoindentation experimental data, indicating key parameters as shown in Fig. 16. The hardness is defined as,

$$H_N = \frac{P_{max}}{A} \quad (6)$$

Where P_{max} is the maximum indentation load and A is the projected contact area at P_{max} which is calculated by the optical sensor present in the nanoindenter. The contact depth h_c is calculated by equation 7 as shown below[65].

$$h_c = h_{max} - \beta \times \frac{P_{max}}{S} \quad (7)$$

where S is the contact stiffness (refer to Fig. 16) which is calculated from the initial slope of the unloading curve at P_{max} . β is a constant that depends on the geometry of the indenter ($\beta = 1.034$ for a sharp Berkovich indenter), and E_r is the reduced modulus which is defined by the following equation.

$$\frac{1}{E_r} = \frac{1-\mu_s^2}{E_s} + \frac{1-\mu_i^2}{E_i} \quad (8)$$

Effects of non-rigid indenters on the load-displacement behaviours can be effectively accounted for by defining a reduced modulus (E_r). μ_s and μ_i are the Poisson's ratios of the samples and the indenter, respectively, and E_s and E_i are the corresponding elastic moduli (for a diamond indenter, E_i is around 1140 GPa and $\mu_i = 0.07$). Reduced elastic modulus E_r is calculated using Equations 9 and 10 as shown below[65]:

$$E_r = \frac{\sqrt{\pi}}{2} \times \frac{S}{\sqrt{A}} \quad (\text{General formula proposed by Oliver Pharr}) \quad (9)$$

$$E_r = \frac{\sqrt{\pi}}{2} \times \frac{S}{\sqrt{24.5 \times h_c}} \quad (\text{Formula for sharp Berkovich/Vickers indenter}) \quad (10)$$

4.4. Microstructure and Composition of the Coated Samples

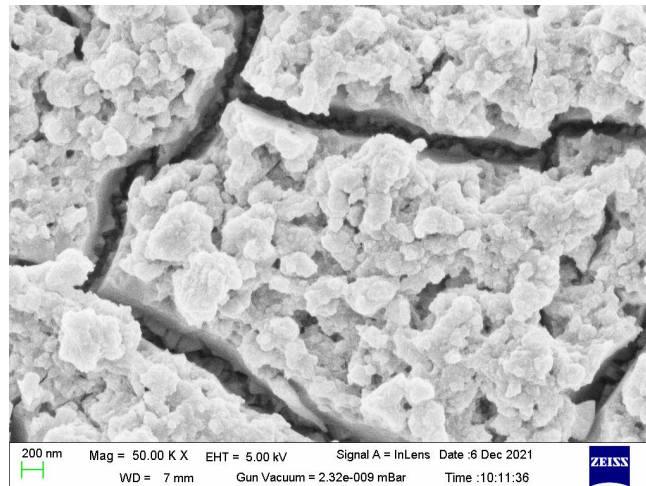


Fig 17a. SEM micrograph of Ni-Co-P coating at 50KX magnification

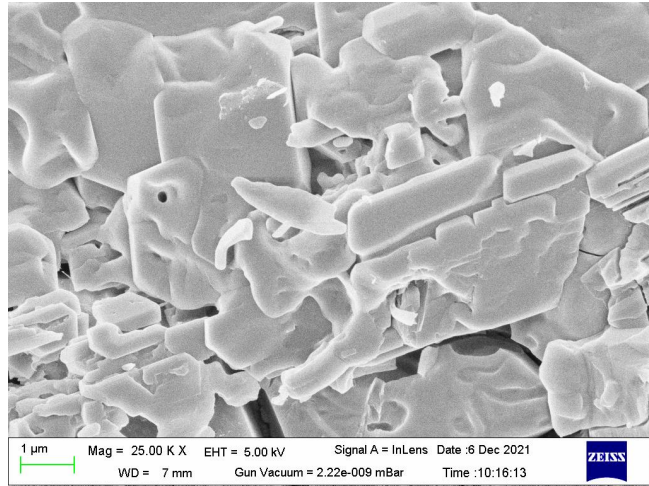


Fig 17b. SEM micrograph of Ni-Co-P coating at 25KX magnification

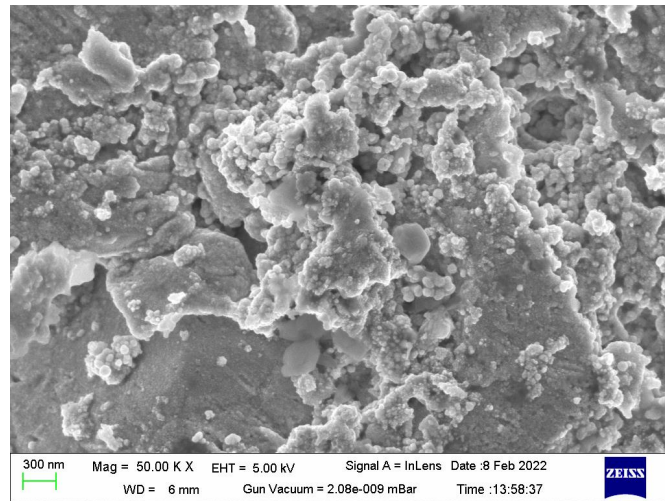


Fig 18a. SEM micrograph of Ni-Mo-P coating at 50KX magnification

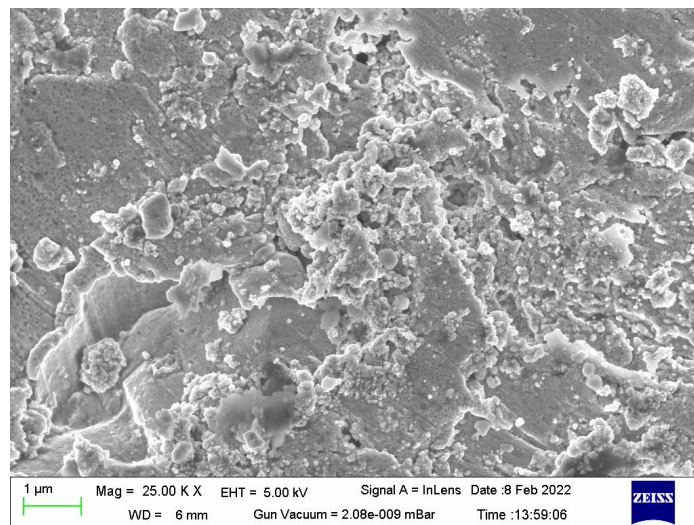


Fig 18b. SEM micrograph of Ni-Mo-P coating at 25KX magnification

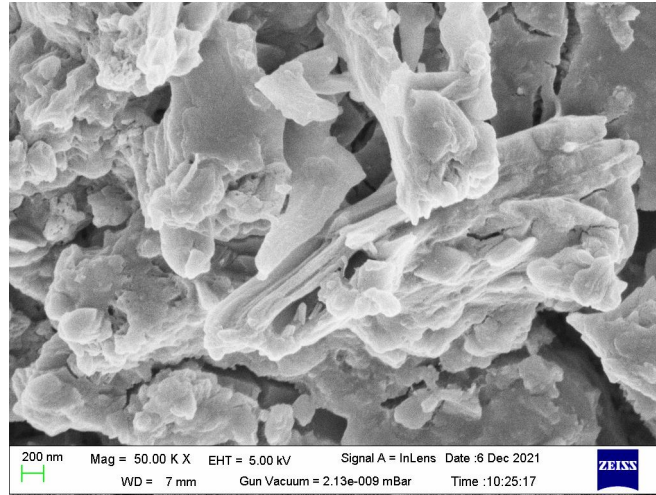


Fig 19a. SEM micrograph of Ni-W-P coating at 50KX magnification

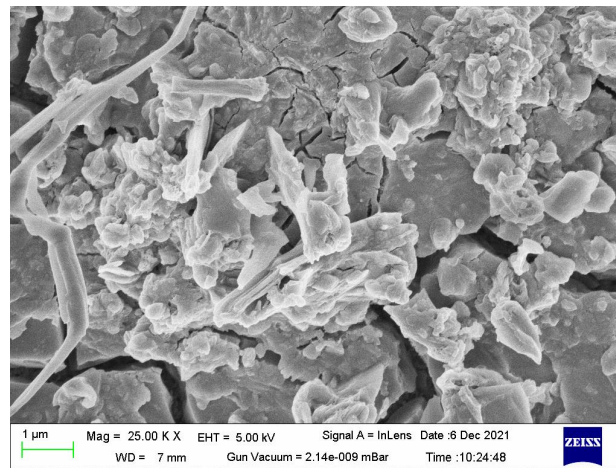


Fig 19b. SEM micrograph of Ni-W-P coating at 25KX magnification

Evaluation of the mechanical properties of thin film is very challenging and hard to predict the actual value. Properties will highly depend upon the composition of the surface which is directly related to the plating method that has been utilized. Not only that, uniformity of the coating is very tough to attain. So, the points which are chosen for evaluating the nanomechanical property of the coating might have different compositions and microstructural orientations. For this reason, to enhance the accuracy of the estimated values, an average of five different indentation results have been taken under consideration. Literature review suggests a huge difference in mechanical properties of the same coating studied by different researchers due to the variation in composition and synthesis methodologies. The bath compositions of the three types of coating have already been discussed and it would be more scientific to analyse the microstructure and composition of the same which has been done by Scanning Electron Microscopy(SEM) and Energy Dispersive X-Ray Spectroscopy(EDS). Fig. 17(a, b), 18(a, b) and 19(a, b) show the SEM image of Ni-Co-P, Ni-Mo-P and Ni-W-P which are taken at same magnification for better comparison. Energy-dispersive X-ray spectroscopy(EDS) results show the composition of the said coatings which is quite satisfactory and the quality of the coating deposition is within the acceptable range(refer to Fig. 20, 21 and 22).

Element	Weight%	Atomic%
P	31.97	47.13
Co	11.31	8.77
Ni	56.71	44.10
Total	100	100

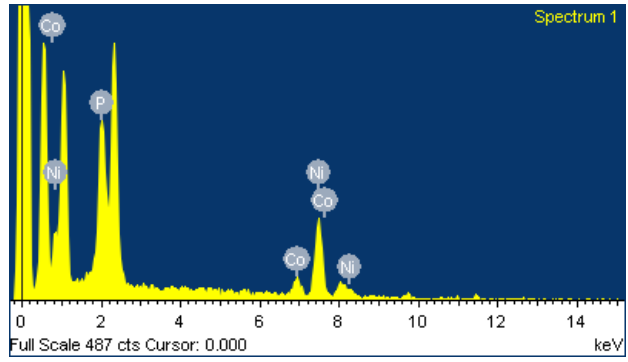


Fig 20. EDS result for showing elemental compositions for Ni-Co-P coating

Element	Weight%	Atomic%
P	1.29	2.60
Ni	80.98	85.89
Mo	17.73	11.51
Total	100	100

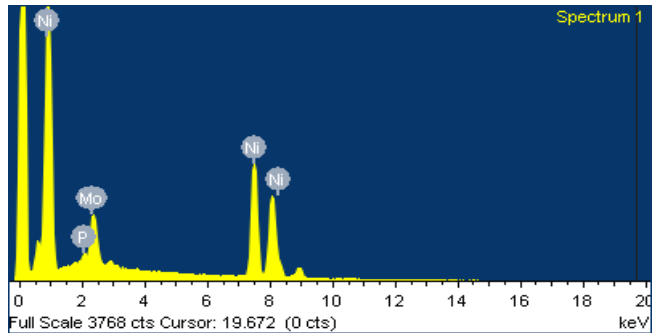


Fig 21. EDS result for showing elemental compositions for Ni-Mo-P coating

Element	Weight%	Atomic%
P	1.42	2.94
Ni	28.84	55.93
W	69.74	41.13
Total	100.00	100

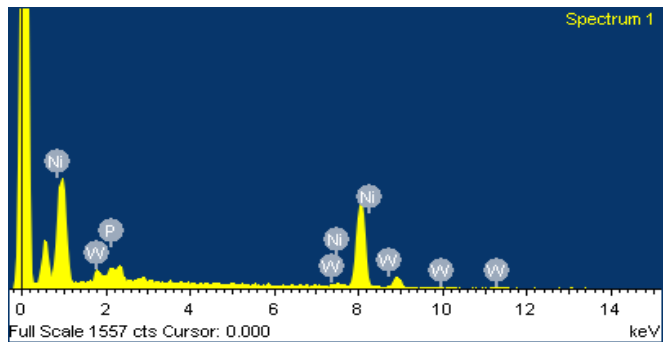


Fig 22. EDS result for showing elemental compositions for Ni-W-P coating

4.5. Result and Discussion

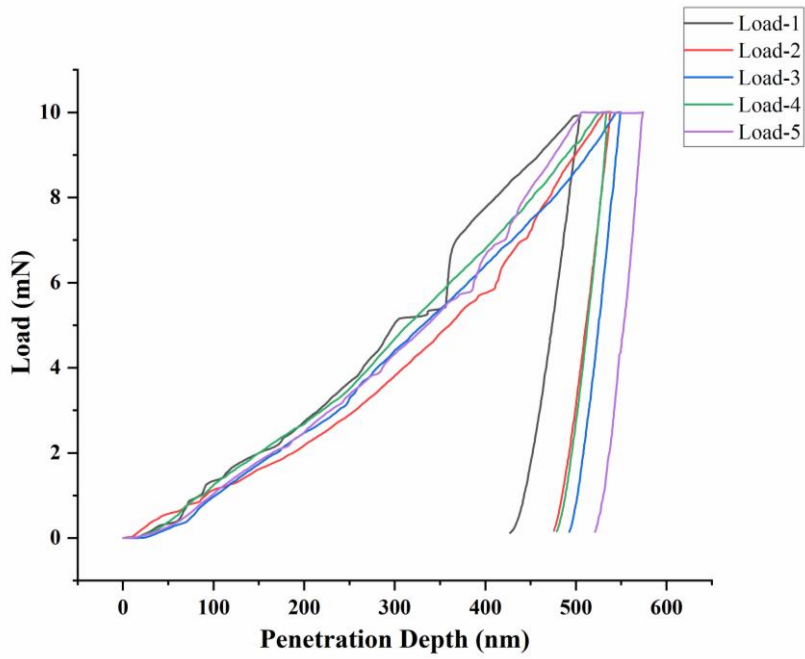


Fig 23. Load vs indenter penetration depth plot for Ni-Co-P coating at five distinct points.

Result for Ni-Mo-P

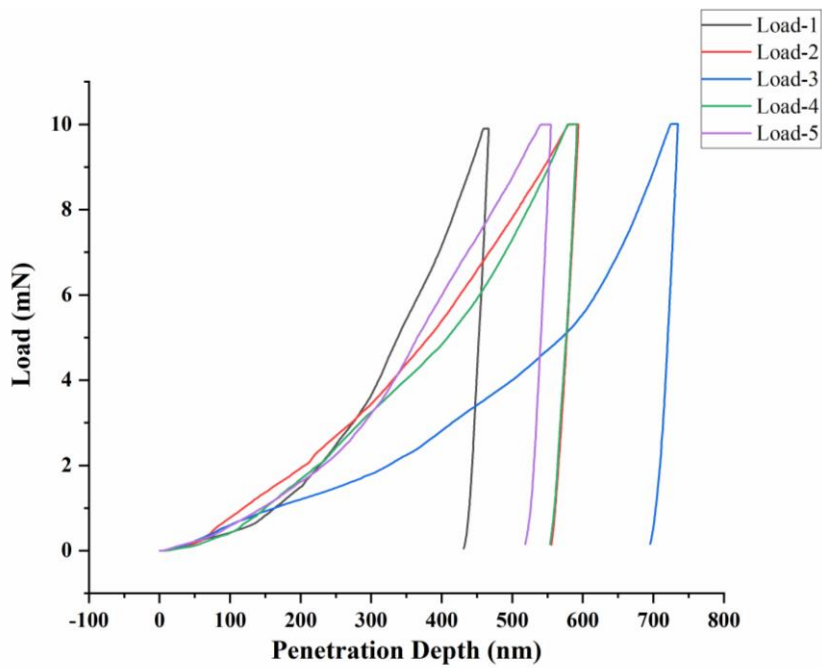


Fig 24. Load vs indenter penetration depth plot for Ni-Mo-P coating at five distinct points.

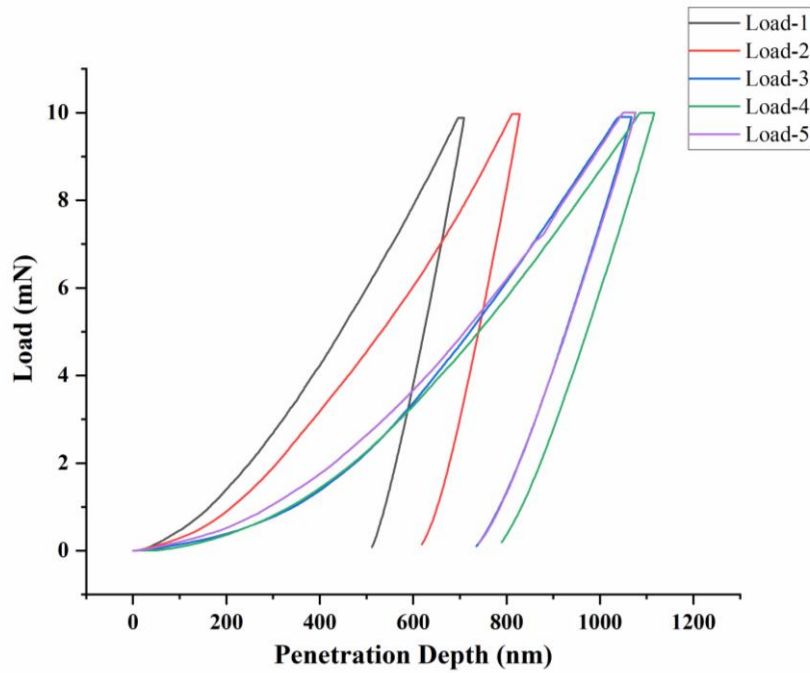


Fig 25. Load vs indenter penetration depth plot for Ni-W-P coating at five distinct points.

Applied load and the penetration depth of the nanoindenter have been plotted for Ni-Co-P, Ni-Mo-P and Ni-W-P in Fig. 23, 24 and 25 respectively. Each figure consists of five test data sets which have been utilized to calculate the initial slope ($S = \frac{dP}{dh}$) of the unloading sections. This value is the key to finding out the elastic modulus of the test sample using the Oliver Pharr model. The values of hardness, elastic modulus and their average values for each of the coated samples are presented in detail in Tables 13, 14 and 15 respectively.

Table 13. Nanoindentation result for Ni-Co-P Coating

Sl. No.	Young's Modulus(GPa)	Nanohardness(MPa)
Run 1	57.902	1598.4
Run 2	61.72	1364.2
Run 3	66.656	1295.3
Run 4	81.342	1312.9
Run 5	90.883	1130.8
Average Value	71.7	1340.32

Table 14. Nanoindentation result for Ni-Mo-P Coating

Sl. No.	Young's Modulus(GPa)	Nanohardness(MPa)
Run 1	139.91	1640.3
Run 2	88.202	1055.3
Run 3	84.423	692.62
Run 4	110.23	1040.6
Run 5	105.92	1202.3

Average Value	105.737	1126.224
----------------------	---------	----------

Table 15. Nanoindentation result for Ni-W-P Coating

Sl. No.	Young's Modulus(GPa)	Nanohardness(MPa)
Run 1	163.68	1006.8
Run 2	137.44	718.64
Run 3	69.486	489.41
Run 4	65.905	449.44
Run 5	67.213	503.85
Average Value	100.75	633.63

From Fig. 23, 24 and 25 it can be concluded that the indentation on each sample is performed with varying penetration depth but the maximum load is kept constant. Penetration depth varies a little bit as the elastic property of the coatings at the microstructural level can change from point to point. Nanoindentation at five different points will reduce the uncertainty in predicting the mechanical properties of the coatings. Cobalt is having the lowest value of Young's modulus(YM) compared to Molybdenum and Tungsten which is fully justified by the average value of YM of Ni-Co-P coating. YM of Mo generally lies below W but the average value of YM for Ni-Mo-P is higher than Ni-W-P. This occurs due to the compositional variation of constituent elements and uneven deposition on the substrate surface. Besides, the selection of indentation points is very crucial as it will affect the results directly. The accuracy of the evaluated properties can further be refined if the number of tests is increased beyond five.

5. Optimization of Corrosion Rate of Ni-Co-P Coating Using Box-Behnken Design and Gradient Descent with RMSprop Algorithm

5.1. Literature review on the Machine Learning Algorithms used for optimization purposes

Copper is broadly used in industrial applications because of its highly desirable mechanical properties, damping capacity, and low cost. With all the desired potential of copper, it still experiences some corrosive problems[98]. In order to avoid or minimize this setback, many techniques have been adopted and employed in the past, amongst which Electroless Nickel (EN) coating has been ascertained to be a great solution. The biggest advantage of EN coating is that it provides a uniform surface finish over the substrate, safeguards the substrate from corrosion, erosion, scratch and wear and enables a surface to exhibit many other desired physical and chemical characteristics[4,24,99]. Different methods can be performed for improving EN coatings viz. alloy coatings, composite coatings, polymer and nanocomposite coatings. As the demand for newer and superior properties of surfaces is increasing day by day, the research in the multipurpose field of coating technologies like electroless, PVD, CVD, sol-

gel, spray coating etc. is spreading rapidly[11,40,100–102]. Apart from that, FEA-based design and modelling of coating and substrate assembly is an emerging area of study as it is capable of predicting design attributes in a very cost-effective way which might be almost impossible to obtain by the experimental study as the thickness of the coating is very less[103–106]. Extensive research works have been done and still going on to assess different surface degradation phenomena and mitigate those using electroless nickel-based coatings. Apart from its several advantages discussed before, it is to be noted that EN coating is a very cost-effective deposition process unlike many other sophisticated plating processes like PVD, CVD etc[107,108]. There are many desirable properties that can be obtained from a coated surface. One of the most important properties is corrosion resistance. Many engineering industries need to use their equipment in a corrosive environment which reduces their life span causing economic loss. Depending upon the condition and nature of the application of a component, it may be subjected to various corrosion like galvanic, pitting, crevice, uniform corrosion etc[109]. From the basic Ni-P coating to various Ni-P based alloy and composite coating have been synthesized so far and found to be very effective to prevent the unwanted corrosion of surfaces leading to failure[49,110,111]. Titanium based nickel coating is found to be very effective to prevent the corrosion of surfaces by Zhi et al[49] while another study by Ram et al[50] confirms that silicon carbide (SiC) and zirconium oxide(ZrO₂) based nanocomposite coating is also an excellent alternative to attain anti-corrosive property on the mild steel surface. The addition of different alloying elements with electroless nickel deposits is also a viable and cheaper option as compared to nanocomposite coatings in order to improve the existing properties including corrosion resistance[100,112,113]. The same has been done in this study where cobalt is added with Ni-P matrix electrolessly. Corrosion behaviour of electroless nickel-phosphorous coatings is predominantly governed by three main factors viz. the degree of amorphous state, the amount of residual stress and the phosphorus content percentage[41,114,115]. The literature review suggests that emphasis has been laid on the research of corrosion resistance of electroless Ni-Co-P coating[116,117]. Studies on the optimization of surface roughness and maximization of micro-hardness of electroless Ni-Co-P have been performed by Sarkar et al[118,119]. Similar type of study on the corrosion resistance of the same in seawater environment has been done by Zhang et al and the process parameters for maximum corrosion resistance is evaluated[120]. Research has also been carried out on multilayer Ni-Co-P coating with variable thickness to improve its sliding wear characteristic[121]. However, there has been a lack of research work on the corrosion rate of electrolessly deposited low cost Ni-Co-P coating and minimizing it with efficient mathematical modelling and machine learning optimizer.

After evaluating a specific characteristic of coating, it is also a very important task to optimize the same and to find the corresponding coating parameters with help of some software packages so that unnecessary wastage of resources is prevented to conduct rigorous experimental works. Response surface methodology(RSM) is a widely accepted analysis method for this purpose for its ease in design and evaluation method. Mathematical modelling and optimization of several coating parameters like hardness, corrosion, wear resistance etc. have been performed using RSM and results are found to be very satisfactory[122–124]. Optimization of Ni-X-P ternary coating properties on both Steel[125] and Aluminium surfaces[124] have been carried out. Shozib et al[124] have compared the mean squared error(MSE) and coefficient of determination(R²) obtained in the various machine learning(ML) techniques that can be used for this purpose. Research has also been done on the optimization of the corrosion rate of the AZ91D magnesium alloy using a support vector machine(SVM) and extreme learning method(ELM) which is important for cardiovascular applications as it is used to manufacture

heart stents[126,127]. It is observed that microhardness optimization of Ni-B with ion concentrations, time and temperature as input parameters using a backpropagation ANN is comparable with BBD optimization[128]. Similar results are obtained for surface finish optimization of Ni-B coating on aluminium substrates using zwitterion concentration as input using backpropagation ANN and Genetic algorithm optimizer[129]. Apart from thermal and wear-resistance coatings, thin-film coatings of ZnO have also been studied and optimized using this method[130]. Nowadays, Artificial Intelligence(AI) and Machine learning(ML) techniques are being used in the diverse areas of research viz optimization of manufacturing processes of electronic equipment like Printed Circuit Boards[131], optimization of solar photovoltaic cells using ML with a knowledge constraint approach[132] and so on. ML techniques have also found their way into the design and optimization of carbon nanotube coatings. Process parameters like argon-acetylene flow rate, hydrogen flow rate and deposition temperature are used as inputs for maximizing the hardness using metaheuristic approaches like Genetic Algorithms (GA) and Particle Swarm Optimization (PSO) using a model generated by Response Surface Methodology(RSM)[132]. A similar approach is taken for the optimization of electrical conductivity of P3HT-CNT composite thin films[133]. Here, we present a literature review of AI/ML optimization techniques used to study various types of coatings using different methods like SVM, ANN, ELM, Random Forest and Extra Trees in a tabular format (refer to Table 16).

Table 16. A Brief Literature Review on the AI/ML techniques for optimization of properties of surface coatings

Subject	Databas e Used	Input	Output	ML Approach and Optimizer	Prediction	Re f
Ni-P coating on Cr12MoV die steel	Experim ental, Taguchi DoE, 16	Temperatur e, Reducing Agent concentration, pH, Lactic Acid concentration	Phosphor us Content	Back Propagation Neural Network (4:10:1) and Particle Swarm Optimizer	MSE = 0.0792	[3]
Ni - P- TiO2 coating on Aluminium Alloy Substrate	Experim ental, Taguchi DoE, 36	Concentrati on of Nickel Sulphate, Sodium Hypophosp hite, Titanium Oxide, Time and Temperatur e	Microhar dness	Support Vector Machine	MSE = 182.2841	[4]
					R2 = 0.8929	
				Back Propagation ANN (5:8:8:1)	MSE = 210.4337	
				Random Forest	R2 = 0.8420	
			Extra Trees	MSE = 155.4733	R2 = 0.9145	
					MSE= 75.3840	

					R2= 0.9447	
				Response Surface Methodology (non ML)	MSE= 269.084	
					R2 = 0.8539	
AZ91D Magnesium alloy coating using Plasma and HVOF methods	Experimental, Taguchi DoE, 12	HVOF and Plasma coating process parameters	Wear Loss	SVM	MSE = 0.0272	[5]
					R2 = 0.9601	
				ELM	MSE = 0.0068	
					R2 = 0.9901	
Electroless composite Nickel-Boron coating on Aluminum Substrate	Experimental, Taguchi DoE, 15	Nickel ion concentration, stabilizer concentration, reducing agent concentration	Microhardness	Back Propagation Neural Network (3:10:1) and GA optimizer	MSE = 34.18	[6]
					R2 = 0.9852	
				BBD	MSE = 20.48	
					R2 = 0.9901	
Electroless composite Nickel-Boron coating on 7075-T6 Aluminum Alloy	Experimental, Taguchi DoE, 10	Surfactant (Amphoteric Zwitterionic) Concentration	Surface Finish	Back Propagation Neural Network (1:5:1), and GA Optimizer	MSE = 5.581e-7	[7]
					R2 = 0.99411	
ZnO thin films	Experimental, Grey Taguchi DoE, 9	Concentration, Pressure, Temperature, Flow Rate	Thickness Roughness Optical Transmittance	Back Propagation ANN (4:8:3)	R= 0.9998	[8]

The objective of this research is to reduce the corrosion rate of the copper substrate with the aid of Ni-Co-P alloy coating and to find the conditions for optimum corrosion rate. Mathematical modelling of the same is done using Box-Behnken Design (BBD) with the help of corrosion data of fifteen samples having varying concentrations of nickel sulfate, cobalt sulfate and bath temperature. Finally, the regression model ($R^2= 0.9673$) obtained from response surface methodology(RSM) is used to optimize CR by Gradient descent with

RMSprop algorithm which is found to be a very fast and accurate ML technique in predicting the minimum possible CR with corresponding electroless bath variables.

5.2. Modelling and Optimization

5.2.1 Response Surface Modelling(BBD)

Table 17: Concentration levels of different variables of Box Behnken Design

Variables	Unit	Parameter	Lower(-1)	Higher(+1)	Mid-point(0)
Cobalt Sulphate	g/L	A	10	20	15
Sodium Hypophosphite	g/L	B	20	30	25
Temperatures	Degree	C	80	90	85

Table 18: 15 set of experimental variables in the Box Behnken Design (BBD) with Corrosion Rate value

Sl. No	Cobalt Sulphate(X1) (gram/ Litre)	Sodium Hypophosphite(X2) (gram/ Litre)	Temperature(X3) (°C)	Corrosion Rate(Z) (µm/Year)
1	10	30	85	1.4120
2	10	20	85	1.5020
3	15	20	90	0.9270
4	20	30	85	1.5500
5	15	25	85	0.5152
6	15	30	90	1.1320
7	15	25	85	0.5120
8	10	25	90	1.5690
9	10	25	80	1.4290
10	20	25	80	1.6520
11	15	30	80	1.3950
12	15	25	85	0.4968
13	20	25	90	1.2897
14	15	20	80	1.6710
15	20	20	85	1.4982

Box-Behnken designs (BBD) is an experimental design for response surface methodology where the three levels of each factor are kept equally spaced and said to be low, high and central points. It considers the central and midpoints of the solution space and is capable of estimating a quadratic design quite accurately. BBD has some limitations due to its poor coverage of

corner points of a nonlinear design space still, it is used widely in solving many optimization problems due to its simplicity and less requirement of experimental data. It is mainly a mathematical modelling process that predicts the response of the function using simulation. In the present study, simulation is done on the coating parameters following the principle that the lesser the constraints in the function better will be the simulated response of the functions. Based on the BBD, a total of 15 samples with uniform size are prepared and coated at different conditions with three different variable factors. This is done so that an optimization study among them can be conducted and conditions for minimum corrosion rate can be approximated using a machining learning optimization tool. The combined effects of three independent variables i.e. Cobalt sulphate, Sodium hypophosphite and temperature have been studied through this process. The independent factor levels are coded as -1 (low), 0 (central point or middle), and 1 (high) as shown in Table 17. Table 18 shows a total of 15 experiments that are conducted with a variation of 3 factors at 3 different levels to fit the model. To establish the importance of the individual process parameters and their interactions, a regression equation is generated. It estimates the correlation between the response and the input process parameters.

5.2.2 Optimization Using Gradient Descent with RMSprop

Gradient descent is a very popular first-order optimization algorithm used for finding the local minimum of a differentiable function. The algorithm works by moving in the direction of the largest gradient i.e. the greatest slope in the neighbourhood of the point on the surface. It travels a fixed amount of distance on the surface per step and this is called the learning rate. Choosing this learning rate is very critical to the working of this algorithm as the minima might be missed if the learning rate is high. While traversing the surface of the plot, it would be beneficial if we could somehow design an algorithm that would take higher steps in regions of a high gradient and smaller steps in regions of low gradients. This way the chance of off-shooting the minima is reduced. Thus, here comes adaptive stepping algorithms like AdaGrad. AdaGrad uses the root mean squared value of all the previous gradients to resize the learning rate appropriately. One disadvantage is that, because it considers the sum of all the previous gradients, the learning rate sometimes becomes too small. RMS prop is a similar tool using a moving root mean square average of the previous gradients. A hyperparameter called momentum is used to combine the squared gradient value of the current iteration with the moving average value of the previous iteration, thus creating a modified moving average as shown in Equations 11 and 12. This is done to prevent the learning rate from exploding in the case of large gradients and from diminishing in the case of smaller ones. Gradient Descent with the help of RMS Prop is a very robust optimization algorithm that can be used for many optimization problems.

$$x_{i+1} = x_i - \eta \times \frac{g_i}{\sqrt{w_i + \epsilon}} \quad (11)$$

$$w_i = \alpha \times w_{i-1} + (1 - \alpha) \times g_i^2 \quad (12)$$

Where x_{i+1} is the modified value of the input variable for the next iteration, $\frac{\eta}{\sqrt{w_i + \epsilon}}$ is the adaptive learning rate, w_i is the moving average and g_i is the gradient value of the current iteration, α is the momentum factor (generally taken as 0.99) and ϵ is a very small positive number. A concise flow chart of the machine learning programme is shown in Fig. 26.

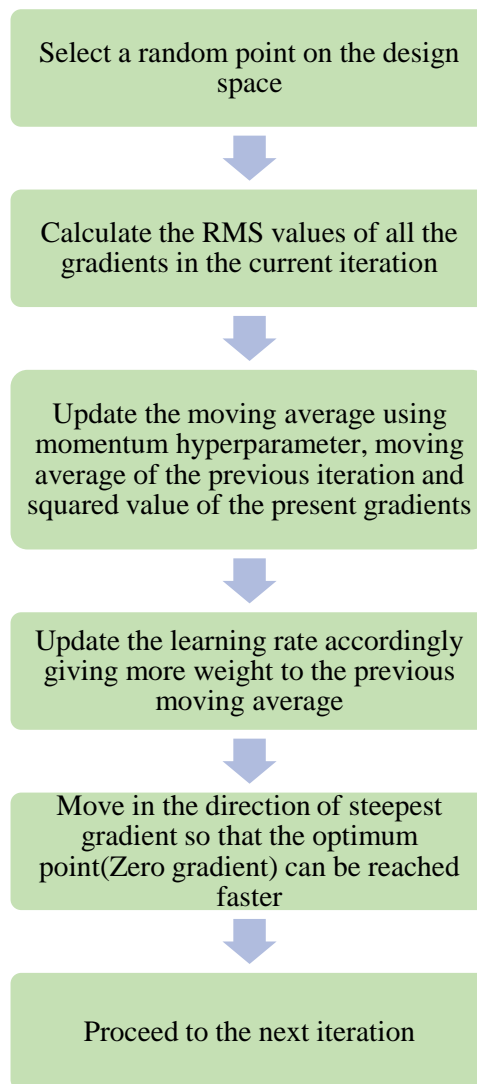


Fig. 26. Flow chart of the python program used to perform optimization using gradient descent with RMSprop

In this study, the optimization process is three parameters based. So, the algorithm is designed accordingly. The first iteration starts with the three random values of sodium hypophosphite, cobalt sulphate and temperature generated by the program itself with the help of the ‘rand’ function. The boundary of the values is entered manually so that the parameters do not go beyond the desired range. The function to be optimized is obtained from the response surface design with the help of fifteen sets of corrosion data obtained experimentally. After 500 iterations, the solution is converged and no further change in the solution is observed even after increasing the number of iterations. The initial step size(η), momentum factor(α), and ϵ are taken as 0.01, 0.99 and 10^{-8} respectively.

5.3. Results

5.3.1 Analysis of variance for response surface

A second or higher-order RSM Model is necessary to approximate the surface around a curvature. In most cases, a second-order RSM model is adequate for this purpose which can be represented by Equation 13.

$$Z = \beta_0 + \sum_{i=1}^k \beta_i X_i + \sum_{i=1}^k \beta_{ii} X_i^2 + \sum_{i=1}^k \sum_{j=1}^k \beta_{ij} X_{ij} + \dots \quad (13)$$

$$Z(\text{Corrosion rate}) = 133.5 - 0.318X_1 - 1.212X_2 - 2.686X_3 + 0.02372X_1^2 + 0.01558X_2^2 + 0.01535X_3^2 + 0.00142X_1X_2 - 0.00502X_1X_3 + 0.00481X_2X_3$$

(14)

The predicted response is influenced by input variables (X_i) and set of regression coefficients: β_0 (intercept coefficient), β_i (linear coefficients), β_{ii} (quadratic coefficients), β_{ij} (interaction coefficients). In this study, X_1 , X_2 , and X_3 are the values of input parameters viz cobalt sulphate, sodium hypophosphite and temperature as shown in Equation 14. It is based on the second-order response surface model (BBD) and approximated by the fifteen sets of experimental data. ANOVA is an effective mathematical tool for determining the significant parameters taking place in a process. It uses the concept of *p-value* and F-value to find significant factors. The *p-value* is a parameter by which we can choose to reject the null hypothesis. If the *p-value* is less than 0.05, the null hypothesis can be rejected or simply we can say that the parameter is significant. In the present case, it shows that the proposed second-order model has a P-value of 0.003 which indicates that it is statistically significant.

Table 19: Statistical results of the ANOVA model

Parameters	Value
Model F-value	16.44
Model P-value	0.003
R-Squared	96.73%
Adj R-Squared	90.85%

The F-value is the ratio of the summation of the square of the factors to the variance of the errors. Hence, a higher value of F will suggest a relatively better factor with respect to others. The results of the ANOVA study of response surface quadratic models for the corrosion rate of the coating are presented in Table 19. It shows the Model is having an F-value of 16.44, implying that the model is significant. As per Table 19, the R-Squared value of the model is 0.9673 which is in reasonable agreement with the Adj R-Squared value (0.9085) as the difference is less than 0.2. Besides, p values of the individual coefficients in Equation 14 are calculated and their contribution to the prediction of corrosion rate is studied. The values including the independent variables X_1 , X_2 , X_3 , interacting variables X_1X_2 , X_2X_3 , X_3X_1 and quadratic variables X_1^2 , X_2^2 , X_3^2 are found to be significant but their contribution levels vary from each other. Among independent variables, temperature (X_3) is found to be most significant having a p-value of 0.019 while for the interacting and quadratic variables, it is X_1X_3 and X_1^2 respectively. Considering the values of ANOVA statistical results for all parameters, the model is found to be well applicable in this work.

5.3.2 Machine Learning Optimization Result

Gradient descent with RMSprop is applied to the multivariable function (Equation 14) obtained from the BBD model as discussed earlier. The partial derivatives with respect to the three variables X_1 , X_2 and X_3 are also required to be provided as input to the python program. The optimum corrosion rate obtained from the machine learning optimizer is 0.435 $\mu\text{m}/\text{Y}$ and the corresponding concentrations of sodium hypophosphite, cobalt sulphate and temperature are found to be 15.06 g/L, 24.93 g/L and 86.049 $^\circ\text{C}$ respectively. So the coating sample having the nearest corresponding composition of 15 g/L, 25 g/L and 85 $^\circ\text{C}$ is considered to be the optimum having a corrosion rate of 0.4968 $\mu\text{m}/\text{Y}$ as found by the corrosion test of the sample. This

signifies that the machine learning optimizer is quite accurate in predicting the value of optimum corrosion rate and corresponding input variables.

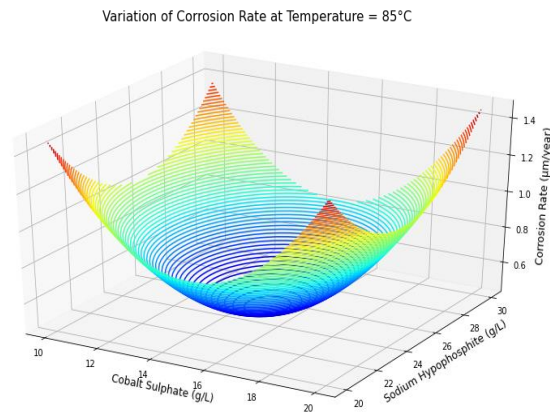


Fig. 27. Second-order 3D surface plot showing the effect of Sodium Hypophosphite and Cobalt Sulphate on corrosion rate

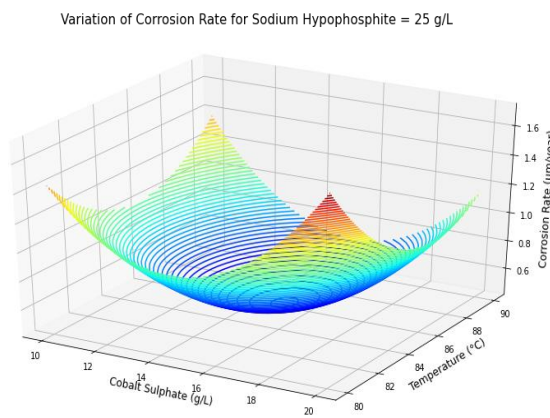


Fig. 28. Second-order 3D surface plot showing the effect of Temperature and Cobalt Sulphate on corrosion rate

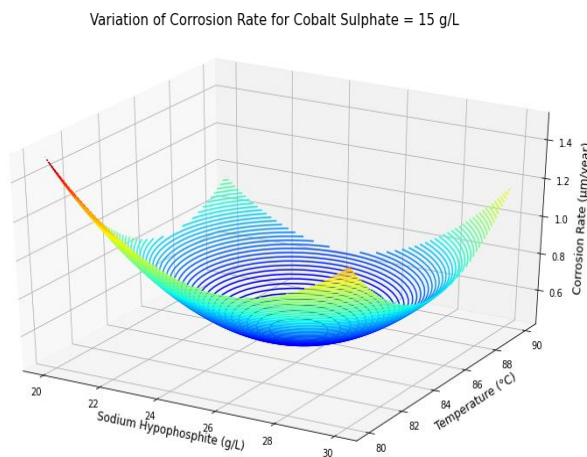


Fig. 29. The second-order 3D surface plot showing the effect of Sodium Hypophosphite and Temperature on corrosion rate

The interactions between the factors can be interpreted from Fig. 27-29 which are plotted by importing the 'matplotlib' library in Jupyter Notebook. Fig. 27 shows the second-order 3D surface plot of the corrosion rate as a function of the concentration of Cobalt sulfate ($\text{CoSO}_4 \cdot 7\text{H}_2\text{O}$) and Sodium Hypophosphite ($\text{NaH}_2\text{PO}_2 \cdot 2\text{H}_2\text{O}$), keeping the temperature constant at 85°C . The plot indicates that the corrosion rate first decreases and then rises with an increase in the concentration of Cobalt sulfate and the concentration of Sodium Hypophosphite. It is symmetric in nature and signifies that both compositions are influencing the corrosion rate equally. Fig. 28 shows the corrosion rate as a function of the concentration of Cobalt sulfate ($\text{CoSO}_4 \cdot 7\text{H}_2\text{O}$) and Temperature *keeping* Sodium Hypophosphite constant at 25g/L. The nature of the plot shows that the Temperature has more influence on corrosion rate compared to Cobalt Sulfate and the same has already been validated by the ANOVA statistical analysis. Lastly, Fig. 29 shows the variation with respect to the concentration of cobalt sulfate ($\text{CoSO}_4 \cdot 7\text{H}_2\text{O}$) and temperature($^\circ\text{C}$) keeping Sodium Hypophosphite($\text{NaH}_2\text{PO}_2 \cdot 2\text{H}_2\text{O}$) constant at 15g/L. It is almost symmetric in nature and has a minima point. It can be inferred that the concentration of Cobalt Sulfate, Sodium Hypophosphite and temperature has a huge influence on the corrosion rate. Observing the surface plots (Fig. 3-5) only, the optimum result can be roughly estimated without the help of an optimization algorithm. From eye estimation, it can be concluded that the minimum corrosion rates likely to occur at around 15 g/L of cobalt sulfate, 25 g/L of sodium hypophosphite and a temperature of 85°C . Under the mentioned conditions, the corrosion rate of the coating is found to be $0.4968\mu\text{m}/\text{Y}$ which matches well with the machine learning result.

6. Conclusion

FEA study is conducted keeping the focus on the design-based analysis of the electroless Ni-P coating in a non-traditional way, unlike the numerous studies on the characterization of the same where the analysis is mainly done on the properties like scratch, wear, hardness, corrosion resistance etc. The uniqueness of this study is that it tries to analyze the coating-substrate assembly in a non-destructive manner. A stainless steel shaft is taken as the substrate as it has a wide application in many mechanical systems making the simulation more realistic and useful for design engineers. The same can also be performed on different types of substrates having simple to complex geometries. Here the FEA is done using a moderate mesh. The result can further be refined using a finer mesh but the nature of the result will be the same. From the four different result files, the zones of maximum and minimum stress, SE, thermal strain, deformation and their nature of distribution over the model can be well approximated. Comparisons of stress and strain energy between the coating and the shaft are performed by evaluating the results along the paths. The induced value of strain energy is discussed in this work as a measure of the stability of an elastic body. The support zones showed the highest gap of SE and σ_e (Path 'D') as it is a highly constrained and most unstable zone. Similarly, the discontinuity values calculated along the other paths (A, B, C) are also found to be in full conformity with the logic used to predict the stability of the coating over the substrate. Hopefully, it can be said that a rigorous study on the FEA-based design and modelling of surface platings will be possible in the near future if all required physical properties of coatings and thin films can be evaluated accurately and cost-effectively.

The main objective of the Nanoindentation study is to evaluate the mechanical properties of Ni-Co-P, Ni-W-P and Ni-Mo-P coatings using nanoindentation loading-unloading data with sufficient accuracy and reliability. Estimation of nanomechanical properties of thin films is very challenging but nanoindentation has been found to be effective and quite accurate in doing so. Average values nanohardness and Young's modulus of three different electroless coatings have been calculated and the values are found to be within the acceptable range. For the particular composition used in our experiment, Ni-Mo-P coating shows the highest value of Young's modulus(105.737 GPa) and Ni-Co-P coating shows the highest value of nanohardness(1340.32 MPa). It is not possible to determine the absolute value of these parameters due to the unpredictability of mechanical properties at the microstructural level and from a point on the coating surface to other points. Uncertainty also arises due to the involvement of three different elements in the deposit and their deposition quality. Though, it can be concluded that nanomechanical characterization of coatings and thin films is possible using precise techniques like nanoindentation and the same can be further refined by increasing the sampling points on the test surface.

Using the machine learning algorithm, the evaluated optimum corrosion rate (0.435 $\mu\text{m}/\text{Y}$) and corresponding process parameters of coating suggested by machine learning are very close to experimental data signifying the optimization to be realistic. It is a decrement of 79.5% from the initial corrosion rate of the bare copper substrate(2.12 $\mu\text{m}/\text{Y}$). ANOVA analysis showed that the effects of cobalt sulfate, temperature and their interaction are significant to influence the corrosion rate of the coating. Prediction and estimation of the surface properties of coatings are still very challenging due to their non-linear and random dependence on synthesis parameters. Machine learning optimization is a cost-effective tool that can be successfully utilized to predict the optimum surface properties and corresponding compositions very accurately eliminating the requirement for repetitive testing. The same has been utilized in this study to determine the optimum corrosion rate of coated surfaces and is found to be a very effective, convenient and rapid decision-making tool.

7. Future Scope

FEA-based analysis is a challenging area and is continuously being modified and upgraded. In the present analysis of Ni-P coating and a stainless steel shaft assembly, FEA is utilized to study the interfacial phenomena occurring at the contacting layer of coating and substrate. This study can further be extended to different types of substrates and coatings but the main challenge will be to evaluate the mechanical properties of the thin film/coating. Another bright area of research in this field is to investigate the design parameters at different locations of the coating-substrate interface practically. But, this will require specially designed instruments to probe a material having a thickness of nano to micrometre order. The feasibility of this delicate study needs to be checked before planning for it. If the experimental validation is possible apart from FEA modelling, its acceptance and versatility will certainly be enhanced.

Nanoindentation is one of the most widely used techniques for the nanomechanical characterization of thin films. As the penetration depth is in the nanometer scale, the measured values from this technique are quite accurate and it does not get influenced by the substrate properties. There are many challenges and opportunities too in this study. To get the accurate surface properties we need to increase the number of indentation points on the coated surface so that all the effects are taken care of properly. Secondly, evaluation of mechanical properties

like Young's modulus for a thin film by this method is not absolutely accurate as the uniformity of the deposition can not always be guaranteed. Besides, the composition of alloy coatings does not remain constant everywhere. People vary the compositions as per the requirement of the surface properties. So, several numbers of indentation studies are possible on different types of alloy coatings with variable compositions. This field is very wide and can be enriched further by the incorporation of algorithms and simulation to predict the mechanical properties of coatings.

The world is going towards a new era where artificial intelligence and machine learning will run the civilization. The process has already been started and will gradually dominate each and every part of human society. Machine learning optimization is a very cost-effective scientific tool as it saves both time and money to a large extent. We can get almost accurate results without installing a huge infrastructure for that. We just need to calibrate the machine initially by a series of test results and then it will work forever without any error in operation. It also requires very minor maintenance. In this present study, the ML algorithm (Gradient Descent with RMSprop) is utilized as a tool to get the electroless bath parameters corresponding to optimum corrosion rate. BBD and CCD design has been utilized extensively in this field and became quite primitive. So the ML algorithm is coupled with the BBD design to get a faster and superior result. There are lots of future scopes in the ML field. Training can be given to a more advanced algorithm like Genetic algorithm, Random Forest and Extra Trees by conducting numerous experiments with variable bath parameters. At the end, we can expect that the ML algorithm will be able to predict the desired surface property at any given electroless bath conditions.

8. References

1. Sudagar J, Lian J, Sha W. Electroless nickel, alloy, composite and nano coatings - A critical review. *J Alloys Compd* [Internet]. 2013;571:183–204. Available from: <http://dx.doi.org/10.1016/j.jallcom.2013.03.107>
2. Sahoo P, Das SK. Tribology of electroless nickel coatings - A review. *Mater Des* [Internet]. 2011;32(4):1760–75. Available from: <http://dx.doi.org/10.1016/j.matdes.2010.11.013>
3. Sarkar S, Kumar Baranwal R, Subhra Sen R, Oraon B, Mukherjee S, Majumdar G. Parametric Optimization of Electroless Ni-P coatings using Taguchi method. *IOP Conf Ser Mater Sci Eng*. 2019;653(1).
4. Shu X, He Z, Wang Y, Yin L. Mechanical properties of Ni-based coatings fabricated by electroless plating method. *Surf Eng* [Internet]. 2020 Sep 1;36(9):944–51. Available from: <https://www.tandfonline.com/doi/full/10.1080/02670844.2019.1662226>
5. Fayyad EM, Abdullah AM, Hassan MK, Mohamed AM, Jarjoura G, Farhat Z. Recent advances in electroless-plated Ni-P and its composites for erosion and corrosion applications: a review. *Emergent Mater* [Internet]. 2018 Jun 15;1(1–2):3–24. Available from: <http://link.springer.com/10.1007/s42247-018-0010-4>
6. Gültekin D, Duru E, Akbulut H. Improved wear behaviors of lead-free electroless Ni B and Ni-B/CeO₂ composite coatings. *Surf Coatings Technol* [Internet]. 2021 Sep;422:127525. Available from: <https://linkinghub.elsevier.com/retrieve/pii/S025789722100699X>
7. Lee S, Kim YY, Cho Y. A comparative study on the elastic characteristics of an

- aluminum thin-film using laser optical measurement techniques. *Coatings*. 2017;7(9).
8. Baranwal RK, Hassan T, Agarwal G, Sarkar S, Majumdar G. Optimization of the stress discontinuity value at the interface of a cylindrical stainless steel substrate and electroless Ni-P coating. *Mater Res Express*. 2019;6(11).
 9. Sribalaji M, Asiq Rahman OS, Laha T, Keshri AK. Nanoindentation and nanoscratch behavior of electroless deposited nickel-phosphorous coating. *Mater Chem Phys* [Internet]. 2016;177(April):220–8. Available from: <http://dx.doi.org/10.1016/j.matchemphys.2016.04.022>
 10. Sarkar S, Baranwal RK, Biswas C, Majumdar G, Haider J. Optimization of process parameters for electroless Ni-Co-P coating deposition to maximize micro-hardness. *Mater Res Express*. 2019;6(4).
 11. Biswas P, Samanta S, Dixit AR, Sahoo RR. Investigation of mechanical and tribological properties of electroless Ni-P-B ternary coatings on steel. *Surf Topogr Metrol Prop* [Internet]. 2021 Sep 1;9(3):035011. Available from: <https://iopscience.iop.org/article/10.1088/2051-672X/ac11c9>
 12. Bonin L, Vitry V. Mechanical and wear characterization of electroless nickel mono and bilayers and high boron-mid phosphorus electroless nickel duplex coatings. *Surf Coatings Technol* [Internet]. 2016;307:957–62. Available from: <http://dx.doi.org/10.1016/j.surfcoat.2016.10.021>
 13. Tima R, Mahboubi F. Effect of plasma nitriding temperature on microstructure and wear properties of electroless nickel-boron coatings. *Surf Coatings Technol* [Internet]. 2021 Jun;415:127084. Available from: <https://linkinghub.elsevier.com/retrieve/pii/S0257897221002589>
 14. Singh S, Samanta S, Das AK, Sahoo RR. Tribological investigation of Ni-graphene oxide composite coating produced by pulsed electrodeposition. *Surfaces and Interfaces* [Internet]. 2018 Sep;12:61–70. Available from: <https://linkinghub.elsevier.com/retrieve/pii/S246802301830244X>
 15. Singh S, Samanta S, Das AK, Sahoo RR. Hydrophobic Reduced Graphene Oxide-Based Ni Coating for Improved Tribological Application. *J Mater Eng Perform* [Internet]. 2019 Jun 24;28(6):3704–13. Available from: <http://link.springer.com/10.1007/s11665-019-04109-9>
 16. Kumar Singh S, Samanta S, Das AK, Sahoo RR. Electrodeposited SiC-graphene oxide composite in nickel matrix for improved tribological applications. *Surf Topogr Metrol Prop* [Internet]. 2019 Jul 16;7(3):035004. Available from: <https://iopscience.iop.org/article/10.1088/2051-672X/ab302d>
 17. Sarkar S, Koley I, Baranwal RK, Mukherjee A, Lamichaney S, Majumdar G. Optimization of process parameters on the response of corrosion resistance of electroless Ni-Co-P coating using Box-Behnken Design (BBD). *J Phys Conf Ser*. 2020;1593(1).
 18. Abubakar AA, Akhtar SS, Arif AFM, Mostaghimi J. The effect of porosity on the hot corrosion failure of thermal barrier coatings. *Model Simul Mater Sci Eng* [Internet]. 2015;23(7):75001. Available from: <http://dx.doi.org/10.1088/0965-0393/23/7/075001>
 19. Van Der Giessen E, Schultz PA, Bertin N, Bulatov V V., Cai W, Csányi G, et al. Roadmap on multiscale materials modeling. *Model Simul Mater Sci Eng*. 2020;28(4).
 20. Bazzaz E, Darvizeh A, Alitavoli M, Tooski MY. Implementation of the new minimum resultant error approach to extract elastic-plastic properties of titanium nitride thin film by nanoindentation, finite element analysis, and modified dimensional analysis. *Proc Inst Mech Eng Part C J Mech Eng Sci*. 2020;234(16):3280–96.
 21. Pearson JD, Zikry MA, Wahl K. Computational design of thin-film nanocomposite coatings for optimized stress and velocity accommodation response. *Wear*.

- 2009;267(5–8):1137–45.
22. Köhler T, Turowski M, Ehlers H, Landmann M, Ristau D, Frauenheim T. Computational approach for structure design and prediction of optical properties in amorphous TiO₂ thin-film coatings. *J Phys D Appl Phys*. 2013;46(32).
 23. Guo S, Li L, Zhang G, Wang W, Zhao X. Stress analysis at the interface between Ni-P coating and SiC p /Al substrate of space mirror. *Appl Surf Sci*. 2009;255(6):3691–5.
 24. Gautam A. Static Stress Analysis of Connecting Rod Using Finite Element Approach. *IOSR J Mech Civ Eng*. 2013;10(1):47–51.
 25. James Prasad Rao B, Srikanth D V., Suresh Kumar T, Sreenivasa Rao L. Design and analysis of automotive composite propeller shaft using fea. *Mater Today Proc* [Internet]. 2016;3(10):3673–9. Available from: <http://dx.doi.org/10.1016/j.matpr.2016.11.012>
 26. Ferrari S, Pellegrino G. FEAfix: FEA Refinement of Design Equations for Synchronous Reluctance Machines. *IEEE Trans Ind Appl*. 2020;56(1):256–66.
 27. Ong SK, Huang JM. Structure design and analysis with integrated AR-FEA. *CIRP Ann - Manuf Technol* [Internet]. 2017;66(1):149–52. Available from: <http://dx.doi.org/10.1016/j.cirp.2017.04.035>
 28. Li W, Noda NA, Sakai H, Takase Y. Thermal stress analysis for shrink fitting system used for ceramics conveying rollers in the process of separation. *Key Eng Mater*. 2011;452–453:241–4.
 29. Reddy PSK, Nagaraju C. Weight optimization and Finite Element Analysis of Composite automotive drive shaft for Maximum Stiffness. *Mater Today Proc* [Internet]. 2017;4(2):2390–6. Available from: <http://dx.doi.org/10.1016/j.matpr.2017.02.088>
 30. Schmidt AA, Schmidt T, Grabherr O, Bartel D. Transient wear simulation based on three-dimensional finite element analysis for a dry running tilted shaft-bushing bearing. *Wear* [Internet]. 2018;408–409:171–9. Available from: <https://doi.org/10.1016/j.wear.2018.05.008>
 31. Afolabi SO, Oladapo BI, Ijagbemi CO, Adeoye AOM, Kayode JF. Design and finite element analysis of a fatigue life prediction for safe and economical machine shaft. *J Mater Res Technol* [Internet]. 2019;8(1):105–11. Available from: <http://dx.doi.org/10.1016/j.jmrt.2017.10.007>
 32. Zhao LH, Xing QK, Wang JY, Li SL, Zheng SL. Failure and root cause analysis of vehicle drive shaft. *Eng Fail Anal* [Internet]. 2019;99(January 2018):225–34. Available from: <https://doi.org/10.1016/j.engfailanal.2019.02.025>
 33. Liu Z, Yu G, He A, Wang L. Simulation of thermal stress in Er₂O₃ and Al₂O₃ tritium penetration barriers by finite-element analysis. *Plasma Sci Technol*. 2017;19(9).
 34. Peng XL, Li XF. Thermal stress in rotating functionally graded hollow circular disks. *Compos Struct* [Internet]. 2010;92(8):1896–904. Available from: <http://dx.doi.org/10.1016/j.compstruct.2010.01.008>
 35. Lei D, Fu X, Ren Y, Yao F, Wang Z. Temperature and thermal stress analysis of parabolic trough receivers. *Renew Energy* [Internet]. 2019;136:403–13. Available from: <https://doi.org/10.1016/j.renene.2019.01.021>
 36. Hawileh RA, Naser MZ. Thermal-stress analysis of RC beams reinforced with GFRP bars. *Compos Part B Eng* [Internet]. 2012;43(5):2135–42. Available from: <http://dx.doi.org/10.1016/j.compositesb.2012.03.004>
 37. Choi W, Fujiyama K, Kim B, Song G. Development of thermal stress concentration factors for life assessment of turbine casings. *Int J Press Vessel Pip* [Internet]. 2012;98:1–7. Available from: <http://dx.doi.org/10.1016/j.ijpvp.2012.07.001>
 38. De Oliveira MCL, Correa OV, Ett B, Sayegh II, de Lima NB, Antunes RA. Influence of

- the tungsten content on surface properties of electroless Ni-W-P coatings. *Mater Res*. 2018;21(1):1–13.
39. Sudagar J, Lian J, Sha W. Electroless nickel, alloy, composite and nano coatings – A critical review. *J Alloys Compd* [Internet]. 2013 Sep;571:183–204. Available from: <https://linkinghub.elsevier.com/retrieve/pii/S0925838813006385>
 40. Fotovvati B, Namdari N, Dehghanhadikolaei A. On Coating Techniques for Surface Protection: A Review. *J Manuf Mater Process* [Internet]. 2019 Mar 25;3(1):28. Available from: <https://www.mdpi.com/2504-4494/3/1/28>
 41. Biswas N, Baranwal RK, Majumdar G, Brabazon D. Review of duplex electroless coatings and their properties. *Adv Mater Process Technol* [Internet]. 2018 Jul 3;4(3):448–65. Available from: <https://www.tandfonline.com/doi/full/10.1080/2374068X.2018.1457298>
 42. Brenner A, Riddell GE. Nickel plating on steel by chemical reduction. *J Res Natl Bur Stand* (1934) [Internet]. 1946 Jul;37(1):31. Available from: https://nvlpubs.nist.gov/nistpubs/jres/37/jresv37n1p31_A1b.pdf
 43. Sankara Narayanan TSN, Selvakumar S, Stephen A. Electroless Ni–Co–P ternary alloy deposits: preparation and characteristics. *Surf Coatings Technol* [Internet]. 2003 Jul;172(2–3):298–307. Available from: <https://linkinghub.elsevier.com/retrieve/pii/S0257897203003153>
 44. Rabizadeh T, Allahkaram SR. Corrosion resistance enhancement of Ni-P electroless coatings by incorporation of nano-SiO₂ particles. *Mater Des* [Internet]. 2011;32(1):133–8. Available from: <http://dx.doi.org/10.1016/j.matdes.2010.06.021>
 45. Zhao Q, Liu Y. Comparisons of corrosion rates of Ni–P based composite coatings in HCl and NaCl solutions. *Corros Sci* [Internet]. 2005 Nov;47(11):2807–15. Available from: <https://linkinghub.elsevier.com/retrieve/pii/S0010938X04003452>
 46. Soleimani R, Mahboubi F, Kazemi M, Arman SY. Corrosion and tribological behaviour of electroless Ni-P/nano-SiC composite coating on aluminium 6061. *Surf Eng*. 2015;31(9):714–21.
 47. Li D, LiDing, Liu Z, Li Q, Guo K, Cao H. Simulation Analysis on Mechanical Property Characterization of Carbon Nanotubes Reinforced Epoxy Composites. *Comput Model Eng Sci* [Internet]. 2020;125(1):145–71. Available from: <https://www.techscience.com/CMES/v125n1/40209>
 48. Soni SK, Thomas B, Kar VR. A Comprehensive Review on CNTs and CNT-Reinforced Composites: Syntheses, Characteristics and Applications. *Mater Today Commun* [Internet]. 2020 Dec;25:101546. Available from: <https://linkinghub.elsevier.com/retrieve/pii/S2352492820325575>
 49. Li Z, Islam MA, Farhat Z. Investigation of Erosion–Corrosion Resistance of Electroless Ni–P–Ti Composite Coatings. *J Bio- Tribo-Corrosion* [Internet]. 2020 Dec 12;6(4):107. Available from: <https://link.springer.com/10.1007/s40735-020-00404-4>
 50. Ram M, Kumar M, Ansari A, Sharma S, Sharma A. Corrosion Resistance of Electroless Ni-P-SiC/ Ni-P-TiO₂-ZrO₂ Nano-Coatings in Paper Mill Bleach Plant. *Mater Today Proc* [Internet]. 2020;21:1200–12. Available from: <https://linkinghub.elsevier.com/retrieve/pii/S2214785320301310>
 51. Kunrath M, dos Santos R, de Oliveira S, Hubler R, Sesterheim P, Teixeira E. Osteoblastic Cell Behavior and Early Bacterial Adhesion on Macro-, Micro-, and Nanostructured Titanium Surfaces for Biomedical Implant Applications. *Int J Oral Maxillofac Implants* [Internet]. 2020 Jul;35(4):773–81. Available from: http://quintpub.com/journals/omi/abstract.php?iss2_id=1693&article_id=20499
 52. Ferraris S, Cochis A, Cazzola M, Tortello M, Scalia A, Spriano S, et al. Cytocompatible and Anti-bacterial Adhesion Nanotextured Titanium Oxide Layer on

- Titanium Surfaces for Dental and Orthopedic Implants. *Front Bioeng Biotechnol* [Internet]. 2019 May 9;7. Available from: <https://www.frontiersin.org/article/10.3389/fbioe.2019.00103/full>
53. Gao Q, Feng T, Huang D, Liu P, Lin P, Wu Y, et al. Antibacterial and hydroxyapatite-forming coating for biomedical implants based on polypeptide-functionalized titania nanospikes. *Biomater Sci* [Internet]. 2020;8(1):278–89. Available from: <http://xlink.rsc.org/?DOI=C9BM01396B>
 54. Bouet G, Cabanettes F, Bidron G, Guignandon A, Peyroche S, Bertrand P, et al. Laser-Based Hybrid Manufacturing of Endosseous Implants: Optimized Titanium Surfaces for Enhancing Osteogenic Differentiation of Human Mesenchymal Stem Cells. *ACS Biomater Sci Eng* [Internet]. 2019 Sep 9;5(9):4376–85. Available from: <https://pubs.acs.org/doi/10.1021/acsbiomaterials.9b00769>
 55. Uddin GM, Jawad M, Ghufraan M, Saleem MW, Raza MA, Rehman ZU, et al. Experimental investigation of tribo-mechanical and chemical properties of TiN PVD coating on titanium substrate for biomedical implants manufacturing. *Int J Adv Manuf Technol* [Internet]. 2019 Jun 7;102(5–8):1391–404. Available from: <http://link.springer.com/10.1007/s00170-018-03244-2>
 56. Peng C, Zhao Y, Jin S, Wang J, Liu R, Liu H, et al. Antibacterial TiCu/TiCuN Multilayer Films with Good Corrosion Resistance Deposited by Axial Magnetic Field-Enhanced Arc Ion Plating. *ACS Appl Mater Interfaces* [Internet]. 2019 Jan 9;11(1):125–36. Available from: <https://pubs.acs.org/doi/10.1021/acsami.8b14038>
 57. Sanderson T. Measuring the elastic moduli of electroless nickel-phosphorus deposits. *Plat Surf Finish*. 2005;92(6):39–43.
 58. Karunaratne MSA, Kyaw S, Jones A, Morrell R, Thomson RC. Modelling the coefficient of thermal expansion in Ni-based superalloys and bond coatings. *J Mater Sci* [Internet]. 2016 May 8;51(9):4213–26. Available from: <http://link.springer.com/10.1007/s10853-015-9554-3>
 59. Hurley DC, Geiss RH, Kopycinska-Müller M, Müller J, Read DT, Wright JE, et al. Anisotropic elastic properties of nanocrystalline nickel thin films. *J Mater Res* [Internet]. 2005 May 3;20(5):1186–93. Available from: <http://link.springer.com/10.1557/JMR.2005.0146>
 60. Zhang F. Ultrasonic Characterization of the Mechanical Properties of Nano-Structured Diamond-Like Carbon Thin Films. In: *AIP Conference Proceedings* [Internet]. AIP; 2005. p. 1159–65. Available from: <http://aip.scitation.org/doi/abs/10.1063/1.1916803>
 61. Lee S, Kim Y, Cho Y. A Comparative Study on the Elastic Characteristics of an Aluminum Thin-Film Using Laser Optical Measurement Techniques. *Coatings* [Internet]. 2017 Sep 10;7(9):143. Available from: <http://www.mdpi.com/2079-6412/7/9/143>
 62. Yan W, Pun CL, Simon GP. Conditions of applying Oliver–Pharr method to the nanoindentation of particles in composites. *Compos Sci Technol* [Internet]. 2012 Jun;72(10):1147–52. Available from: <https://linkinghub.elsevier.com/retrieve/pii/S026635381200125X>
 63. Chakraborty H, Sinha A, Mukherjee N, Ray D, Protim Chattopadhyay P. A study on nanoindentation and tribological behaviour of multifunctional ZnO/PMMA nanocomposite. *Mater Lett* [Internet]. 2013 Feb;93:137–40. Available from: <https://linkinghub.elsevier.com/retrieve/pii/S0167577X12016497>
 64. Tsongas K, Tzetzis D, Karantzalis A, Baniias G, Exarchos D, Ahmadkhaniha D, et al. Microstructural, Surface Topology and Nanomechanical Characterization of Electrodeposited Ni-P/SiC Nanocomposite Coatings. *Appl Sci* [Internet]. 2019 Jul 19;9(14):2901. Available from: <https://www.mdpi.com/2076-3417/9/14/2901>

65. Ozmetin AE, Sahin O, Ongun E, Kuru M. Mechanical characterization of MgB₂ thin films using nanoindentation technique. *J Alloys Compd* [Internet]. 2015 Jan;619:262–6. Available from: <https://linkinghub.elsevier.com/retrieve/pii/S0925838814021495>
66. Oliver WC, Pharr GM. An improved technique for determining hardness and elastic modulus using load and displacement sensing indentation experiments. *J Mater Res* [Internet]. 1992 Jun;7(6):1564–83. Available from: <http://link.springer.com/10.1557/JMR.1992.1564>
67. Jung YG, Lawn BR, Martyniuk M, Huang H, Hu XZ. Evaluation of elastic modulus and hardness of thin films by nanoindentation. *J Mater Res*. 2004;19(10):3076–80.
68. Zhang W, Li J, Xing Y, Nie X, Lang F, Yang S, et al. Experimental Study on the Thickness-Dependent Hardness of SiO₂ Thin Films Using Nanoindentation. *Coatings* [Internet]. 2020 Dec 27;11(1):23. Available from: <https://www.mdpi.com/2079-6412/11/1/23>
69. Sribalaji M, Asiq Rahman OS, Laha T, Keshri AK. Nanoindentation and nanoscratch behavior of electroless deposited nickel-phosphorous coating. *Mater Chem Phys* [Internet]. 2016 Jul;177:220–8. Available from: <https://linkinghub.elsevier.com/retrieve/pii/S0254058416302310>
70. Weikert T, Wartzack S, Baloglu MV, Willner K, Gabel S, Merle B, et al. Evaluation of the surface fatigue behavior of amorphous carbon coatings through cyclic nanoindentation. *Surf Coatings Technol* [Internet]. 2021 Feb;407:126769. Available from: <https://linkinghub.elsevier.com/retrieve/pii/S0257897220314390>
71. Vardanyan VH, Urbassek HM. Strength of Graphene-Coated Ni Bi-Crystals: A Molecular Dynamics Nano-Indentation Study. *Materials (Basel)* [Internet]. 2020 Apr 4;13(7):1683. Available from: <https://www.mdpi.com/1996-1944/13/7/1683>
72. Vitry V, Delaunois F, Dumortier C. Mechanical properties and scratch test resistance of nickel–boron coated aluminium alloy after heat treatments. *Surf Coatings Technol* [Internet]. 2008 Apr;202(14):3316–24. Available from: <https://linkinghub.elsevier.com/retrieve/pii/S0257897207012273>
73. Oh I-H, Lee J-Y, Han J-K, Lee H-J, Lee B-T. Microstructural characterization of Al₂O₃–Ni composites prepared by electroless deposition. *Surf Coatings Technol* [Internet]. 2005 Mar;192(1):39–42. Available from: <https://linkinghub.elsevier.com/retrieve/pii/S0257897204003263>
74. Balaraju JN, Seshadri SK. Preparation and Characterization of Electroless Ni-P and Ni-P-Si₃N₄ Composite Coatings. *Trans IMF* [Internet]. 1999 Jan 8;77(2):84–6. Available from: <https://www.tandfonline.com/doi/full/10.1080/00202967.1999.11871253>
75. Taheri R, Oguocha IN., Yannacopoulos S. The tribological characteristics of electroless NiP coatings. *Wear* [Internet]. 2001 Jun;249(5–6):389–96. Available from: <https://linkinghub.elsevier.com/retrieve/pii/S0043164801005397>
76. Staia MH, Castillo EJ, Puchi ES, Lewis B, Hintermann HE. Wear performance and mechanism of electroless Ni–P coating. *Surf Coatings Technol* [Internet]. 1996 Dec;86–87:598–602. Available from: <https://linkinghub.elsevier.com/retrieve/pii/S0257897296030861>
77. Jiaqiang G, Lei L, Yating W, Bin S, Wenbin H. Electroless Ni–P–SiC composite coatings with superfine particles. *Surf Coatings Technol* [Internet]. 2006 May;200(20–21):5836–42. Available from: <https://linkinghub.elsevier.com/retrieve/pii/S0257897205010340>
78. Sahoo P. Wear behaviour of electroless Ni–P coatings and optimization of process parameters using Taguchi method. *Mater Des* [Internet]. 2009 Apr;30(4):1341–9. Available from: <https://linkinghub.elsevier.com/retrieve/pii/S0261306908003002>

79. Sahoo P, Das SK. Tribology of electroless nickel coatings – A review. *Mater Des* [Internet]. 2011 Apr;32(4):1760–75. Available from: <https://linkinghub.elsevier.com/retrieve/pii/S0261306910006394>
80. Karunaratne MSA, Kyaw S, Jones A, Morrell R, Thomson RC. Modelling the coefficient of thermal expansion in Ni-based superalloys and bond coatings. *J Mater Sci*. 2016;51(9):4213–26.
81. Hurley DC, Geiss RH, Kopycinska-Müller M, Müller J, Read DT, Wright JE, et al. Anisotropic elastic properties of nanocrystalline nickel thin films. *J Mater Res*. 2005;20(5):1186–93.
82. Zhang F, Krishnaswamy S, Fei D, Rebinsky DA. Ultrasonic characterization of the mechanical properties of nano-structured diamond-like carbon thin films. *AIP Conf Proc*. 2005;760:1159–65.
83. Huh YH, Kim DI, Kim DJ, Lee HM, Hong SG, Park JH, et al. Measurement of mechanical properties of thin film by membrane deflection test. *Exp Mech*. 2010;50(4):429–35.
84. Kinast J, Hilpert E, Rohloff RR, Gebhardt A, Tünnermann A. Thermal expansion coefficient analyses of electroless nickel with varying phosphorous concentrations. *Surf Coatings Technol* [Internet]. 2014;259(PC):500–3. Available from: <http://dx.doi.org/10.1016/j.surfcoat.2014.10.038>
85. Kim J-H, Yeon S-C, Jeon Y-K, Kim J-G, Kim Y-H. Nano-indentation method for the measurement of the Poisson's ratio of MEMS thin films. *Sensors Actuators A Phys* [Internet]. 2003 Nov;108(1–3):20–7. Available from: <https://linkinghub.elsevier.com/retrieve/pii/S0924424703003613>
86. Wei Z, Zhang G, Chen H, Luo J, Liu R, Guo S. A simple method for evaluating elastic modulus of thin films by nanoindentation. *J Mater Res* [Internet]. 2009 Mar 31;24(3):801–15. Available from: <http://link.springer.com/10.1557/jmr.2009.0126>
87. Martan J, Čapek J, Chalhoub EA. Measurement of thermal properties of thin films up to high temperatures — Pulsed photothermal radiometry system and Si – B – C – N films Measurement of thermal properties of thin films up to high temperatures — Pulsed photothermal radiometry system and Si. 2013;124902(2010).
88. Yoshiizumi M, Oikawa N, Shimada K, Endo S, Sugiyama M, Mikami H, et al. Thermal Conductivity Evaluation of Polymer Thin Film. 2013;559:555–9.
89. Queen DR, Hellman F. Thin film nanocalorimeter for heat capacity measurements of 30 nm films. 2012;063901(2009).
90. Ruoho M, Valset K, Finstad T, Tittonen I. Measurement of thin film thermal conductivity using the laser flash method. 2015;26.
91. Science M, Sciences L. Determination of the Modulus of Elasticity , Poissons Ratio and the Coefficient. 2014;(December).
92. Thompson RJ, Hemker KJ. Thermal expansion measurements on coating materials by digital image correlation. *Proc SEM Annu Conf Expo Exp Appl Mech* 2007. 2007;2(January 2007):1058–67.
93. Xu H, Cuevas-maraver J, Kevrekidis G, Vainchtein A. An energy-based stability criterion for solitary travelling waves in Hamiltonian lattices *Subject Areas* : 2018;
94. Rohrlich F. Self-Energy and Stability of the Classical Electron. *Am J Phys*. 1960;28(7):639–43.
95. Saville RM, Rakshe S, Haagenen JAJ, Shukla S, Spormann AM. Energy-dependent stability of *Shewanella oneidensis* MR-1 biofilms. *J Bacteriol*. 2011;193(13):3257–64.
96. Han X, Liu M, Huang H, Tan B. Electrostatic Balance Parameter Mediated Energy Functions-Toward the Stability and Performance of Explosives. *Propellants, Explos Pyrotech* [Internet]. 2021 Aug 22;46(8):1313–23. Available from:

- <https://onlinelibrary.wiley.com/doi/10.1002/prop.202100027>
97. Shustova NB, Cozzolino AF, Dinca M. Conformational Locking by Design: Relating Strain Energy with Luminescence and Stability in Rigid Metal – Organic Frameworks. 2012;8–11.
 98. Lin C-K, Hsu C-H, Cheng Y-H, Ou K-L, Lee S-L. A study on the corrosion and erosion behavior of electroless nickel and TiAlN/ZrN duplex coatings on ductile iron. *Appl Surf Sci* [Internet]. 2015 Jan;324:13–9. Available from: <https://linkinghub.elsevier.com/retrieve/pii/S0169433214023071>
 99. Abo-Zahhad EM, Ookawara S, Radwan A, El-Shazly AH, El-Kady MF, Esmail MFC. Performance, limits, and thermal stress analysis of high concentrator multijunction solar cell under passive cooling conditions. *Appl Therm Eng* [Internet]. 2020;164:114497. Available from: <https://doi.org/10.1016/j.applthermaleng.2019.114497>
 100. Shibli SMA, Chinchu KS. Development and electrochemical characterization of Ni-P coated tungsten incorporated electroless nickel coatings. *Mater Chem Phys* [Internet]. 2016 Aug;178:21–30. Available from: <https://linkinghub.elsevier.com/retrieve/pii/S025405841630253X>
 101. Croll SG. Surface roughness profile and its effect on coating adhesion and corrosion protection: A review. *Prog Org Coatings* [Internet]. 2020 Nov;148:105847. Available from: <https://linkinghub.elsevier.com/retrieve/pii/S0300944020306111>
 102. Srikanth A, Mohammed Thalib Basha G, Venkateshwarlu B. A Brief Review on Cold Spray Coating Process. *Mater Today Proc* [Internet]. 2020;22:1390–7. Available from: <https://linkinghub.elsevier.com/retrieve/pii/S2214785320305873>
 103. Zhang XC, Xu BS, Wang HD, Wu YX, Jiang Y. Effects of compositional gradient and thickness of coating on the residual stresses within the graded coating. *Mater Des* [Internet]. 2007 Jan;28(4):1192–7. Available from: <https://linkinghub.elsevier.com/retrieve/pii/S0261306906000276>
 104. Guo S, Li L, Zhang G, Wang W, Zhao X. Stress analysis at the interface between Ni-P coating and SiCp/Al substrate of space mirror. *Appl Surf Sci* [Internet]. 2009 Jan;255(6):3691–5. Available from: <https://linkinghub.elsevier.com/retrieve/pii/S0169433208021442>
 105. Luo JF, Liu YJ, Berger EJ. Interfacial stress analysis for multi-coating systems using an advanced boundary element method. *Comput Mech* [Internet]. 2000 Jan 20;24(6):448–55. Available from: <http://link.springer.com/10.1007/s004660050004>
 106. Baranwal RK, Hassan T, Agarwal G, Sarkar S, Majumdar G. Optimization of the stress discontinuity value at the interface of a cylindrical stainless steel substrate and electroless Ni-P coating. *Mater Res Express* [Internet]. 2019 Sep 27;6(11):116421. Available from: <https://iopscience.iop.org/article/10.1088/2053-1591/ab431c>
 107. Barati Q, Hadavi SMM. Electroless Ni-B and composite coatings: A critical review on formation mechanism, properties, applications and future trends. *Surfaces and Interfaces* [Internet]. 2020 Dec;21:100702. Available from: <https://linkinghub.elsevier.com/retrieve/pii/S2468023020306945>
 108. Jana A, Roy S, Bose GK, Sarkar S. Electroless Coating on Non-Conductive Materials. In 2021. p. 188–208. Available from: <http://services.igi-global.com/resolvedoi/resolve.aspx?doi=10.4018/978-1-7998-4870-7.ch008>
 109. Ahmad Z. TYPES OF CORROSION. In: *Principles of Corrosion Engineering and Corrosion Control* [Internet]. Elsevier; 2006. p. 120–270. Available from: <https://linkinghub.elsevier.com/retrieve/pii/B9780750659246500052>
 110. Jian S-Y, Chang J-K, Lin K-F, Chen T-Y, Yuan J-H, Ger M-D. Characteristic V-Mn conversion coating in reinforcing corrosion resistance of electroless Ni-P coated LZ91

- Mg alloy. *Surf Coatings Technol* [Internet]. 2020 Jul;394:125724. Available from: <https://linkinghub.elsevier.com/retrieve/pii/S0257897220303935>
111. Liu B, Zhang Q, Li Y, Yang Y, Zhang T, Wang Y, et al. Optimization of the Corrosion Resistance of Electroless Ni–W–P Coatings on Magnesium Alloys by the Response Surface Methodology. *Coatings* [Internet]. 2020 Dec 25;11(1):18. Available from: <https://www.mdpi.com/2079-6412/11/1/18>
 112. Faraji S, Rahim AA, Mohamed N, Sipaut CS, Raja B. Corrosion resistance of electroless Cu–P and Cu–P–SiC composite coatings in 3.5% NaCl. *Arab J Chem* [Internet]. 2013 Oct;6(4):379–88. Available from: <https://linkinghub.elsevier.com/retrieve/pii/S1878535210002194>
 113. Abdel-Gawad SA, Sadik MA, Shoeib MA. Preparation and properties of a novel nano Ni-B-Sn by electroless deposition on 7075-T6 aluminum alloy for aerospace application. *J Alloys Compd* [Internet]. 2019 May;785:1284–92. Available from: <https://linkinghub.elsevier.com/retrieve/pii/S0925838819302476>
 114. Ma H, Tian F, Li D, Guo Q. Study on the nano-composite electroless coating of Ni–P/Ag. *J Alloys Compd* [Internet]. 2009 Apr;474(1–2):264–7. Available from: <https://linkinghub.elsevier.com/retrieve/pii/S0925838808010220>
 115. Song YW, Shan DY, Han EH. High corrosion resistance of electroless composite plating coatings on AZ91D magnesium alloys. *Electrochim Acta* [Internet]. 2008 Jan;53(5):2135–43. Available from: <https://linkinghub.elsevier.com/retrieve/pii/S0013468607011607>
 116. Gao Y, Huang L, Zheng ZJ, Li H, Zhu M. The influence of cobalt on the corrosion resistance and electromagnetic shielding of electroless Ni–Co–P deposits on Al substrate. *Appl Surf Sci* [Internet]. 2007 Oct;253(24):9470–5. Available from: <https://linkinghub.elsevier.com/retrieve/pii/S016943320700788X>
 117. Shi LT, Hu J, Fang L, Wu F, Liao XL, Meng FM. Effects of cobalt content on mechanical and corrosion properties of electroless Ni-Co-P/TiN nanocomposite coatings. *Mater Corros* [Internet]. 2016 Oct;67(10):1034–41. Available from: <https://onlinelibrary.wiley.com/doi/10.1002/maco.201608844>
 118. Sarkar S, Baranwal RK, Biswas C, Majumdar G, Haider J. Optimization of process parameters for electroless Ni–Co–P coating deposition to maximize micro-hardness. *Mater Res Express* [Internet]. 2019 Jan 18;6(4):046415. Available from: <https://iopscience.iop.org/article/10.1088/2053-1591/aafc47>
 119. Sarkar S, Mukherjee A, Kumar Baranwal R, De J, Biswas C, Majumdar G. Prediction and parametric optimization of surface roughness of electroless Ni-Co-P coating using Box-Behnken design. *J Mech Behav Mater* [Internet]. 2019 Dec 24;28(1):153–61. Available from: <https://www.degruyter.com/document/doi/10.1515/jmbm-2019-0017/html>
 120. Zhang Y, Kang M, Yao L, Mbugua NS, Jin M, Zhu J. Study on the Wear and Seawater Corrosion Resistance of Ni–Co–P Alloy Coatings with Jet Electrodeposition in Different Jet Voltages and Temperatures of Plating Solution. *Coatings* [Internet]. 2020 Jun 30;10(7):639. Available from: <https://www.mdpi.com/2079-6412/10/7/639>
 121. Karimzadeh A, Rouhaghdam AS, Aliofkhaezrai M, Miresmaeili R. Sliding wear behavior of Ni–Co–P multilayer coatings electrodeposited by pulse reverse method. *Tribol Int* [Internet]. 2020 Jan;141:105914. Available from: <https://linkinghub.elsevier.com/retrieve/pii/S0301679X19304335>
 122. Oraon B, Majumdar G, Ghosh B. Improving hardness of electroless Ni–B coatings using optimized deposition conditions and annealing. *Mater Des* [Internet]. 2008 Jan;29(7):1412–8. Available from: <https://linkinghub.elsevier.com/retrieve/pii/S0261306907002142>

123. Chelladurai SJS, K. M, Ray AP, Upadhyaya M, Narasimharaj V, S. G. Optimization of process parameters using response surface methodology: A review. *Mater Today Proc* [Internet]. 2021;37:1301–4. Available from: <https://linkinghub.elsevier.com/retrieve/pii/S2214785320349440>
124. Shozib IA, Ahmad A, Rahaman MSA, Abdul-Rani A majdi, Alam MA, Beheshti M, et al. Modelling and optimization of microhardness of electroless Ni–P–TiO₂ composite coating based on machine learning approaches and RSM. *J Mater Res Technol* [Internet]. 2021 May;12:1010–25. Available from: <https://linkinghub.elsevier.com/retrieve/pii/S2238785421002908>
125. Zou XF, Hu YJ, Long XB, Huang LY. Prediction and optimization of phosphorus content in electroless plating of Cr12MoV die steel based on PSO-BP model. *Surfaces and Interfaces* [Internet]. 2020 Mar;18:100443. Available from: <https://linkinghub.elsevier.com/retrieve/pii/S2468023019302548>
126. Gurgenc T, Altay O, Ulas M, Ozel C. Extreme learning machine and support vector regression wear loss predictions for magnesium alloys coated using various spray coating methods. *J Appl Phys* [Internet]. 2020 May 14;127(18):185103. Available from: <http://aip.scitation.org/doi/10.1063/5.0004562>
127. Gu XN, Zhou WR, Zheng YF, Cheng Y, Wei SC, Zhong SP, et al. Corrosion fatigue behaviors of two biomedical Mg alloys – AZ91D and WE43 – In simulated body fluid. *Acta Biomater* [Internet]. 2010 Dec;6(12):4605–13. Available from: <https://linkinghub.elsevier.com/retrieve/pii/S1742706110003466>
128. Vijayanand M, Varahamoorthi R, Kumaradhas P, Sivamani S. Modelling and optimisation of hardness in citrate stabilised electroless nickel boron (ENi-B) coatings using back propagation neural network – Box Behnken design and simulated annealing – genetic algorithm. *Trans IMF* [Internet]. 2021 Sep 3;99(5):253–64. Available from: <https://www.tandfonline.com/doi/full/10.1080/00202967.2021.1898172>
129. Vijayanand M, Varahamoorthi R, Kumaradhas P, Sivamani S, Kulkarni M V. Regression-BPNN modelling of surfactant concentration effects in electroless Ni B coating and optimization using genetic algorithm. *Surf Coatings Technol* [Internet]. 2021 Mar;409:126878. Available from: <https://linkinghub.elsevier.com/retrieve/pii/S0257897221000517>
130. Kumari N, Gohel J V., Patel SR. Multi-response optimization of ZnO thin films using Grey-Taguchi technique and development of a model using ANN. *Optik (Stuttg)* [Internet]. 2017 Sep;144:422–35. Available from: <https://linkinghub.elsevier.com/retrieve/pii/S0030402617307763>
131. Wankerl H, Stern ML, Mahdavi A, Eichler C, Lang EW. Parameterized reinforcement learning for optical system optimization. *J Phys D Appl Phys* [Internet]. 2021 Jul 29;54(30):305104. Available from: <https://iopscience.iop.org/article/10.1088/1361-6463/abfddb>
132. Liu Z, Rolston N, Flick AC, Colburn T, Ren Z, Dauskardt RH, et al. Machine Learning with Knowledge Constraints for Process Optimization of Open-Air Perovskite Solar Cell Manufacturing. 2021 Sep 30; Available from: <http://arxiv.org/abs/2110.01387>
133. Bash D, Cai Y, Chellappan V, Wong SL, Xu Y, Kumar P, et al. Machine learning and high-throughput robust design of P3HT-CNT composite thin films for high electrical conductivity. 2020 Nov 20; Available from: <http://arxiv.org/abs/2011.10382>